PLOS GENETICS

RESEARCH ARTICLE

A *C. elegans* Zona Pellucida domain protein functions via its ZPc domain

Jennifer D. Cohen[1], **Jessica G. Bermudez**[2], **Matthew C. Good**[2,3], **Meera V. Sundaram**[1] *

1 Department of Genetics, University of Pennsylvania Perelman School of Medicine, Philadelphia, Pennsylvania, United States of America, **2** Department of Bioengineering, University of Pennsylvania, Philadelphia, Pennsylvania, United States of America, **3** Department of Cell and Developmental Biology, University of Pennsylvania Perelman School of Medicine, Philadelphia, Pennsylvania, United States of America

* sundaram@pennmedicine.upenn.edu

Abstract

Zona Pellucida domain (ZP) proteins are critical components of the body's external-most protective layers, apical extracellular matrices (aECMs). Although their loss or dysfunction is associated with many diseases, it remains unclear how ZP proteins assemble in aECMs. Current models suggest that ZP proteins polymerize via their ZPn subdomains, while ZPc subdomains modulate ZPn behavior. Using the model organism *C. elegans*, we investigated the aECM assembly of one ZP protein, LET-653, which shapes several tubes. Contrary to prevailing models, we find that LET-653 localizes and functions via its ZPc domain. Furthermore, we show that ZPc domain function requires cleavage at the LET-653 C-terminus, likely in part to relieve inhibition of the ZPc by the ZPn domain, but also to promote some other aspect of ZPc domain function. *In vitro*, the ZPc, but not ZPn, domain bound crystalline aggregates. These data offer a new model for ZP function whereby the ZPc domain is primarily responsible for matrix incorporation and tissue shaping.

Author summary

Apical extracellular matrices line and shape external body surfaces and the insides of biological tubes. Common components of apical matrices are Zona Pellucida domain (ZP) proteins. These proteins are typically thought to form fibrillar polymers via their N-terminal ZPn subdomains, but how they do so *in vivo*, and whether other assembly mechanisms occur, is not well understood. Here we use the model organism *C. elegans* to investigate how one ZP protein, LET-653, assembles into a matrix layer. We visualized the matrix assembly of the LET-653 ZP domain *in vivo* and demonstrated that, unlike previously described ZP proteins, LET-653 functions and incorporates into matrix via its C-terminal ZPc subdomain. This study identifies new mechanisms by which ZP proteins can assemble into matrices.

Introduction

The apical extracellular matrices (aECMs) that line the insides, or lumens, of biological tubes are critical for shaping and maintaining tube structure [1]. For example, the aECM of the blood vasculature, the glycocalyx, prevents capillary loss [2]. The surfactant that lines the lung's narrow tubes decreases surface tension to prevent alveoli collapse [3]. Loss or dysfunction of aECMs are associated with a number of human diseases [2, 4, 5].

Despite aECMs' importance in human health, we know little about aECM assembly. aECMs are complex meshworks of glycoproteins, glycosaminoglycans, proteoglycans, lipids, and lipoproteins [1–5]. Individual aECM components can sometimes form insoluble fibrils or water-trapping gels *in vitro* [6–11], but how different components come together *in vivo* is more challenging to decipher. Luminal aECMs are usually difficult to visualize *in vivo* because they are translucent and their structures can be destroyed under desiccating fixation conditions [12]. Where aECMs have been observed, they often form multi- layered structures [12, 13]. For example, the vascular aECM may be up to several microns thick and contains at least three layers with distinct electron density [2, 12]. Generating an aECM requires inhibiting assembly of its various components until after secretion, and then encouraging assembly with appropriate partners at the right time and place. Defects in any of these regulatory steps could disrupt aECM organization and contribute to disease.

Zona Pellucida domain, or ZP, proteins are a widespread and abundant aECM protein family [14]. ZP proteins were originally identified as the major components of the mammalian oocyte's extracellular coat, also called the Zona Pellucida [15]. ZP proteins were later discovered within many somatic aECMs, including those of the kidney tubules (Umod [9], Oit3 [16]), inner ear (Tecta, Tectb [17]), gut (GP2 [18], DMBT3 [19]) and vasculature (Endoglin [20], Betaglycan [21]). Loss or dysfunction of these ZP proteins is associated with many human diseases, including chronic kidney disease, deafness, and hereditary hemorrhagic telangiectasia (HHT) [19–27]. Several ZP proteins are thought to act primarily by trapping ligands and affecting signaling processes [28, 29], but many form fibrils or aggregates that may play structural roles within the aECM [8, 9, 30, 31]. How ZP proteins assemble into complex extracellular matrix structures *in vivo* is poorly understood.

Although originally described as a single domain, ZP domains are now recognized to contain two separate domains, ZPn and ZPc, that are usually, but not always, found in tandem [32]. Crystal structures reveal that ZPn and ZPc domains independently take on Immunoglobulin (Ig)-like folds held in place by disulfide bonds between paired cysteines [28, 29, 33]. ZPn domains typically have four evenly spaced cysteines, while ZPc domains can have four, six, or eight cysteines with some variability in spacing [30, 34]. ZPc domains are usually followed by a furin-type consensus cleavage site (CCS), then a hydrophobic C-terminus, and sometimes a transmembrane domain or GPI anchor.

Several ZPn domains can polymerize spontaneously to form fibrils *in vitro*, but functions for ZPc domains are less well defined [35–40]. Studies of two non-polymerizing ZP proteins, Endoglin and Betaglycan, suggest that ZPc domains can dimerize and may mediate other protein-protein interactions [28, 29]. However, due to challenges in expressing ZPc domains in cell culture [35, 41], the roles or polymerization capabilities of ZPc domains independent of ZPn domain have not been assessed.

A prevailing model has been that ZPc domains serve as negative regulators of ZPn polymerization. *In vivo*, an external hydrophobic patch (EHP) C-terminal to the CCS is generally required for ZP protein secretion [42–44], and cleavage at the CCS occurs prior to matrix

incorporation [45, 46]. Structural data showed that the EHP is part of the ZPc fold [33], and suggested a model in which ZPn polymerization is inhibited prior to secretion via an intramolecular interaction with the ZPc domain and the C-terminus [35, 44]. This interaction may be stabilized by binding between the EHP and an internal hydrophobic patch (IHP) in the linker between the ZPn and ZPc domains [44, 47]. Under this model, cleavage at the CCS evicts the EHP and C-terminus, releases ZPc-mediated inhibition, and enables ZPn polymerization [44, 48]. However, this model is based on *in vitro* studies of only a few proteins, most of which were modified to promote efficient secretion [30, 49]. It remains unclear whether the ZPc and C-terminus have roles other than facilitating ZPn secretion and assembly, and if and how the ZPn and ZPc domains impact one another's function *in vivo*.

ZP proteins are important structural components of cuticle and other aECMs in invertebrates, including *Caenorhabditis elegans* and *Drosophila* [14, 50]. *C. elegans* has an unusually large set of ZP proteins [34], many of which affect shaping of specific epithelia [51–59]. Furthermore, *C. elegans* is genetically tractable and is transparent, allowing live imaging of the aECM [60]. These features make *C. elegans* a particularly attractive model for studying ZP structure/function relationships and matrix assembly.

Here, we investigate the matrix assembly of the *C. elegans* ZP protein LET-653, which shapes multiple tube types. We identify the ZPc domain as the critical domain for LET-653 function and matrix localization and discover that cleavage is required for ZPc function. We also show that the isolated ZPc domain incorporates into aggregates *in vitro*. Together, these data offer a novel model for ZP protein function and matrix assembly.

Results

Background: LET-653 is a luminal ZP protein that shapes the duct and vulva tubes

LET-653 (Fig 1A) is a component of a transient pre-cuticular luminal matrix that shapes multiple developing tubes [52, 61]. LET-653 is essential to shape the tiny excretory duct tube, a unicellular tube that is less than a micron in diameter [52]. All *let-653* mutants die as young larvae due to discontinuities in this tube lumen that prevent fluid excretion (Fig 1B) [52, 62]. *let-653* mutants rescued in the duct cell survive into adulthood, but show more subtle defects in the shaping of other epithelial tissues, including the vulva, which is a large multicellular tube that, in adulthood, serves as the passageway through which embryos are laid [51, 52, 61] (Fig 1E). The excretory duct tube provides the most sensitive assay for LET-653 function, while both the duct (Fig 1C and 1D) and the vulva (Fig 1E–1G) allow rapid visual assessment of matrix incorporation via imaging of fluorescently-tagged LET-653 proteins in live animals.

Previously, we demonstrated that the LET-653 ZP domain is responsible for both tube shaping and incorporation into a membrane anchored aECM [52, 61]. LET-653 is a secreted protein with two N-terminal PAN/Apple (plasminogen) domains and a C-terminal ZP domain [63] (Fig 1A). The PAN and ZP domains each confer different patterns of matrix localization, but only the ZP domain is capable of rescuing *let-653* mutant lethality and both duct and vulva tube shape defects [52, 61]. As observed for most other ZP proteins, the LET-653 C-terminus is cleaved, though LET-653 has no transmembrane or membrane association domain [52]. The cleaved C-terminus stays associated with the rest of the ZP domain *in vivo*, such that tagging LET-653(ZP) at either the N- or C-terminus yields the same localization pattern [52]. Fluorescence recovery after photobleaching (FRAP) analyses indicated that LET-653(ZP) has low mobility, consistent with matrix incorporation [52].
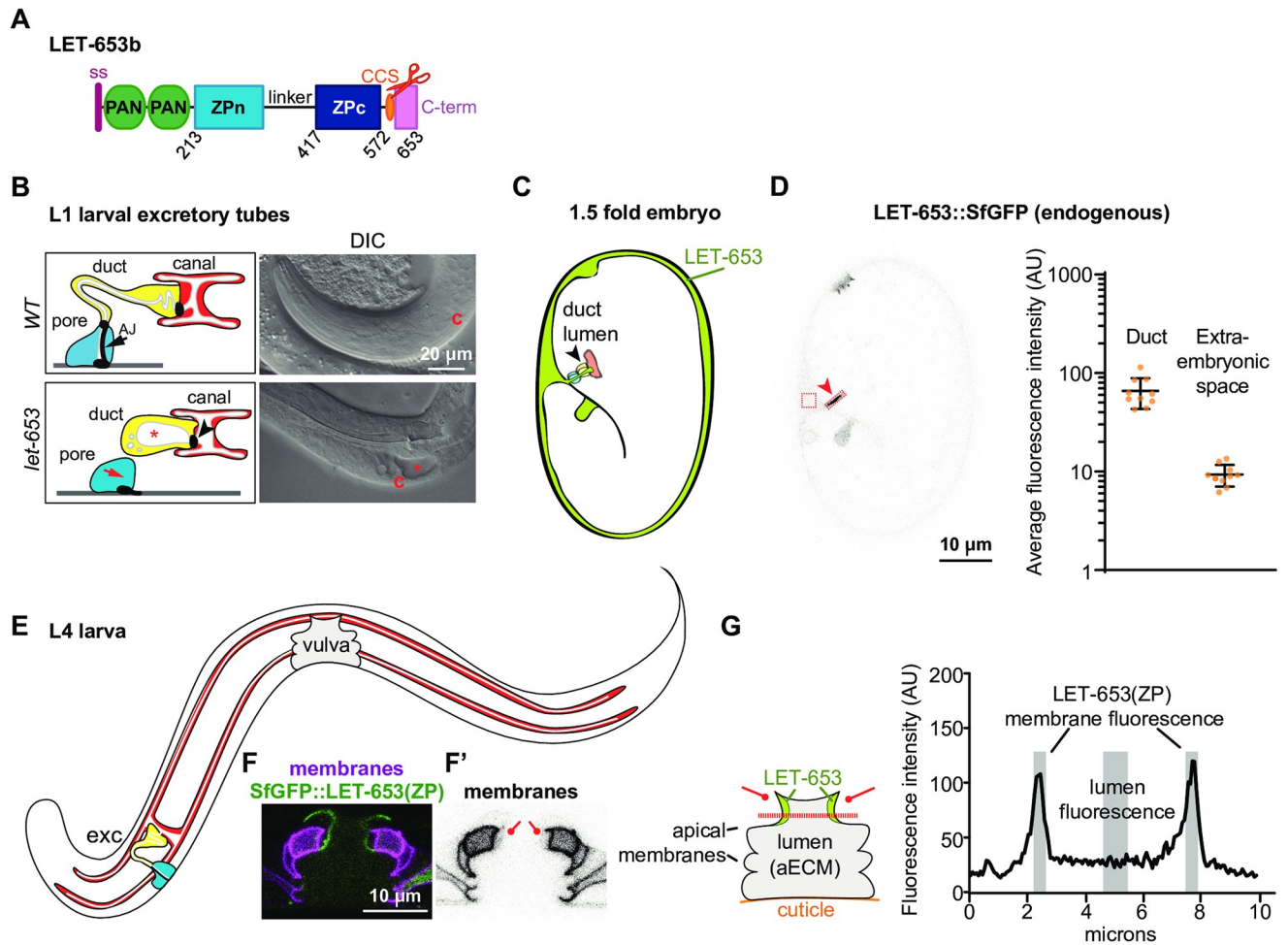
Fig 1. LET-653 is a luminal ZP protein that shapes *C. elegans* tubes. A) Diagram of LET-653 isoform b, on which all structure/function constructs were based. LET-653 has an N-terminal signal peptide (ss, pink) but lacks any other membrane-association domain. PAN; PAN/Apple domains, which are also found in the blood clotting factor plasminogen [81]. CCS (orange oval and scissors); consensus furin-type cleavage site (RRYR) located after the ZP domain and before the C-terminus. The linker is predicted to be N- glycosylated and heavily O-glycosylated. Pink box represents C-terminus. The LET-653 ZP domain aligns well with other ZP proteins, but has several unusual features. The ZPn domain lacks a key tyrosine residue thought to be important for ZPn polymerization [41, 52], and the linker region between the ZP subdomains is unusually long, a feature whose impact is unclear [34]. B) Cartoons of the duct and pore cells of the excretory system and DIC images of *let-653* mutants and *WT C. elegans* at L1 stage. Yellow; duct cell. Blue; pore cell. White; lumen. Black; cell junctions. Asterisk; luminal dilation. c; canal cell nucleus. B) Diagram of *C. elegans* 1.5 fold embryo. White; embryo. Gray; extraembryonic space. Arrowhead indicates duct/pore lumen. Red; canal cell. Yellow; duct cell. Blue; pore cell. D) Confocal image of a 1.5 fold embryo with CRISPR-tagged full-length LET-653::SfGFP [61] with quantification of duct and extraembryonic fluorescence intensity. LET-653 is enriched in the duct lumen (arrowhead), buccal cavity and rectum. Fluorescence intensity was calculated within the indicated boxes to estimate matrix incorporation and overall expression levels, respectively. SfGFP alone shows minimal duct lumen fluorescence but strong extraembryonic fluorescence [52], while endogenously tagged full-length LET-653 shows strong duct lumen fluorescence but minimal extraembryonic fluorescence [61]. Quantification of average endogenous LET-653 fluorescence intensity per pixel in boxes drawn within the duct lumen and extraembryonic space. n = 10. AU; Arbitrary units. Error bars represent standard error. E) Cartoon of L4 larva. F-F') Confocal images of the vulva apical membranes, marked by PH::mCherry, and LET-653(ZP), which lines the dorsal vulE and vulF membranes. F') vulE and vulF membranes are faintly labelled by PH::mCherry (lines). G) Cartoon of vulva lumen and quantification of LET-653 fluorescence. The lumen is lined by 22 cells whose apical membranes define lumen shape. Cuticle lines the base of the vulva and a membranous hymen covers the top, generating a closed tube. Drawing a line across the dorsal region of the vulva allows quantification of LET-653 membrane vs. luminal localization. LET-653 fluorescence across the dashed line shows two peaks near the apical membranes and decreased fluorescence in the center of the lumen. Black; LET-653 fluorescence. Gray; membrane-associated and luminal regions whose fluorescence intensities were averaged. A line of 10 pixels thick (0.63 microns) was drawn across the vulva in the position indicated in panel H. Fluorescence intensity from 5 points proximal to each apical membrane (10 values total) were averaged and divided by the average fluorescence intensity across 10 points from the center of the vulva lumen. AU; arbitrary units.

LET-653 functions via the ZPc domain

Transgenic structure/function experiments were performed to dissect ZP domain aECM assembly and tube shaping function. ZP domain fragments were expressed under a 2.2 kb *let-653* promoter fragment and tagged with Superfolder GFP (SfGFP) [52, 64]. These transgenes were expressed at levels comparable to endogenous, SfGFP-tagged LET-653 as assessed by fluorescence levels (Fig 1D, S1 Fig). For each transgene, multiple independent lines were tested in three assays. To determine function, we tested the ability of transgenes to restore viability to *let-653(cs178)* null mutants (Fig 1B). To assay localization, we imaged the developing duct tube in 1.5 fold embryos (Fig 1C and 1D), and the developing vulva tube in L4 larvae (Fig 1F and 1G). In such assays, the positive control LET-653(ZP) localized transiently to the excretory duct lumen (Fig 2A, S2 Fig) and along specific apical membranes within the vulva tube (Figs 1F and 1G and 2A).

To determine which part of the LET-653 ZP domain is functionally important, we first expressed constructs containing either the ZPn domain and linker or the ZPc domain and C-terminal tail (referred to henceforth as simply ZPn or ZPc). Both proteins were efficiently secreted, but LET-653(ZPn) was expressed at slightly lower levels than LET-653(ZPc) in embryos (Fig 2B–2E). The ZPn domain transgene did not rescue *let-653* mutant lethality (Fig 2F). This protein localized weakly to the duct lumen and had no specific localization in the vulva (Fig 2B, 2D and 2E). In contrast, LET-653(ZPc) rescued *let-653* mutants (Fig 2F). This protein robustly lined the duct and vulva lumens (Fig 2C–2E). These data indicate that LET-653(ZPc) is sufficient for both function and proper localization, and suggest that this domain binds to a partner that helps recruit it to the membrane-anchored matrix.

To test whether the observed function and localization were due to activity of the main part of the ZPc domain or to the C-terminal tail that follows the CCS, we attempted to express each segment independently. The LET-653 C-terminus contains a hydrophobic region that may correspond to an EHP (Fig 3A). To generate a truncated ZPc construct, we removed most (42/78 amino acids) of the C-terminus, leaving only this short, hydrophobic region (Fig 3A and 3B). LET-653(ZPc-½Cterm) was not secreted and did not rescue *let-653* mutant duct defects (Fig 3B and 3D). This is consistent with prior results showing that the C-terminus is required for secretion of LET-653(full ZP)-containing proteins, though not for secretion of LET-653 (ZPn) ([52]; Fig 2B). We conclude that the full C-terminus is required for proper trafficking and secretion of the ZPc domain.

Next, we tested if the LET-653 C-terminus was sufficient for function or localization. Our attempts to make transgenic animals expressing only the LET-653 C-terminal tail failed, suggesting that the C-terminal tail is toxic, perhaps due to its hydrophobicity (Fig 3A). Instead, to test C-terminus activity, we attached it to the ZPn domain (Fig 3C). This resulted in a secreted protein that did not rescue *let-653* mutant duct defects and did not localize to the duct lumen (Fig 3C and 3D). In the vulva, most LET-653(ZPn+Cterm) protein formed large, irregular clumps, but some of the protein localized along the vulva apical membrane (Fig 3C). These observations suggest that the C-terminus does have some capacity for aggregation and/or matrix binding. However, the full ZPc domain is required for tube shaping and appropriate apical matrix localization.

LET-653 cleavage promotes ZPc function

Because ZP cleavage is thought to promote ZPn polymerization, we examined how it impacts LET-653(ZP) function. To test the role of cleavage in LET-653, we mutated the best candidate furin cleavage site (CCS) from RRYR to AAYA in a transgene encoding the full ZP domain (Fig 4A and 4B). Western blotting confirmed that, unlike wild-type LET-653, the mutated
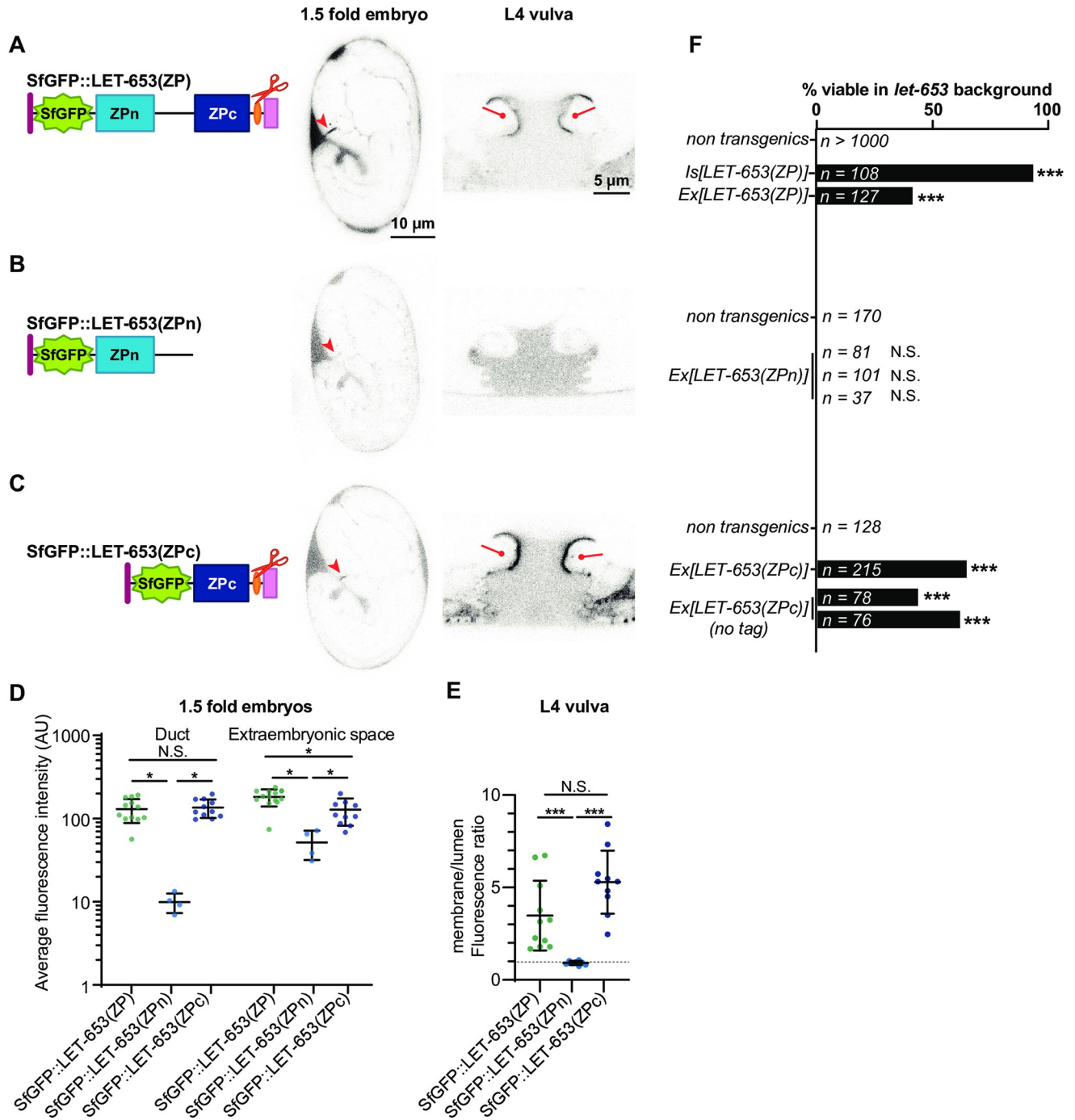
Fig 2. The ZPc domain is necessary and sufficient for LET-653 function. Here and in all subsequent figures, cartoons depict the LET-653 fragments tested and the location of the SfGFP tag (green). A) Full ZP domain. SfGFP::LET-653(ZP) is consistently visible in the duct lumen of 1.5-fold embryos (arrowhead) and along the dorsal apical membranes of the L4 vulva (lines). B) ZPn domain, including the linker. SfGFP::LET-653(ZPn) was occasionally observed in the 1.5 fold duct lumen, but never lined the vulva apical membranes. C) ZPc domain, including the C-terminus (Cterm). SfGFP::LET-653(ZPc) consistently lined the duct lumen and the vulva dorsal apical membranes (lines). D) Duct and extraembryonic fluorescence in 1.5 fold embryos were quantified as shown in Fig 1. Duct fluorescence levels were generally similar to levels of endogenous, full-length LET-653 (Fig 1D), although there were far greater levels of extraembryonic fluorescence, indicating overexpression and/or ectopic localization. p values generated using a two tailed Mann Whitney U test. Duct fluorescence: SfGFP::LET-653(ZP) vs SfGFP::LET-653(ZPc), p = 0.7399. SfGFP::LET-653(ZP) vs SfGFP::LET-653(ZPn), *p = 0.0011. SfGFP:: LET-653(ZPn) vs SfGFP::LET-653(ZPc), *p = 0.0015. Extraembryonic fluorescence: SfGFP::LET-653(ZP) vs SfGFP::LET-653(ZPc), *p = 0.0086. SfGFP:: LET-653(ZP) vs SfGFP::LET-653(ZPn), *p = 0.0011. SfGFP::LET-653(ZPn) vs SfGFP::LET-653(ZPc), *p = 0.0029. Error bars; standard error. E) Ratio of apical membrane-associated to lumen fluorescence in the L4 vulva (see Fig 1). ***p<0.0001, Mann Whitney two-tailed U test. Dashed line indicates a ratio

of 1, where membrane fluorescence is equal to luminal fluorescence. Error bars; standard error. F) Both integrated (Is) and extrachromosomal (Ex) transgenes containing LET-653(ZP) rescued *let-653* mutant lethality. Non-transgenic animals are pooled siblings from experiments in each group; non-transgenic animals never survive. 0/3 independent transgenic lines containing LET-653(ZPn) were functional, but 3/3 lines containing LET-653(ZPc) (either with or without an SfGFP tag) were functional. ***p<0.0001, two-tailed Fisher's Exact test.
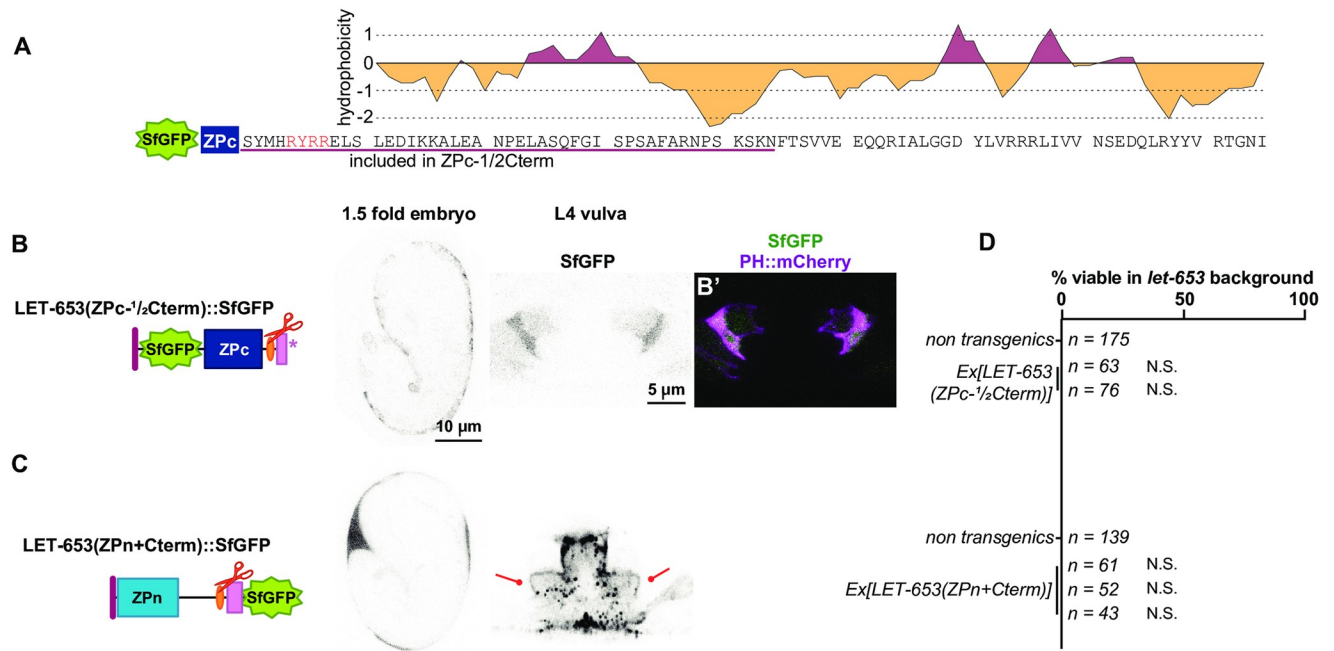
Fig 3. The LET-653 C-terminus confers aggregation activity but is not sufficient for function. A) Diagram of the LET-653 C-terminus. Cleavage site is shown in red. Potential external hydrophobic region (EHP); pink underline. Hydrophobicity plot generated using Kyte and Doolittle algorithm [82]. B) SfGFP::LET-653(ZPc-½Cterm) is truncated after the region underlined in pink in A. LET-653(ZPc-½Cterm) was not secreted. Absence of LET-653 from the duct, extraembryonic space, and vulva lumen was assessed visually via epifluorescence microscopy (n = 20 each). B') Overlay with SfGFP::LET-653 (ZPc-½Cterm) and the membrane marker PH::mCherry, indicating all SfGFP::LET-653(ZPc-½Cterm) is enclosed in membrane. C) LET-653(ZPn +Cterm)::SfGFP. The entire C-terminus, starting at the end of the ZPc subdomain, was added to the end of the ZPn domain. Although efficiently secreted, LET-653(ZPn+Cterm) was rarely observed in the embryonic duct lumen (3/20 embryos) and had a punctate appearance in the vulva lumen (n = 10). Some LET-653(ZPn+Cterm) lined vulva apical membranes (lines). As LET-653(ZPn+Cterm) had punctate localization, its enrichment at the vulva membrane vs. the center of the vulva lumen was not quantified. D) Two independent transgenes containing LET-653(ZPc-½Cterm), and three transgenes containing LET-653(ZPn+Cterm), were non-functional in *let-653* mutants. N.S., not significant, p>0.01, two-tailed Fisher's Exact test.

LET-653(ZP, AAYA) protein is not cleaved in *C. elegans* embryos (Fig 4F). Although this uncleavable protein still localized to the duct lumen, it localized weakly, or not at all, to the apical membrane in the vulva lumen (Fig 4B–4D), and was unable to rescue *let-653* mutant lethality (Fig 4E). LET-653(ZP, AYAA) was expressed at similar levels and cleared from the duct lumen at the same time as the wild-type ZP domain (Fig 4C, S2 Fig), indicating that differences in stability or clearance do not account for these results. We conclude that cleavage promotes LET-653(ZP) function and localization.

To determine how cleavage enables LET-653(ZP) function, we mutated the cleavage site in a transgene expressing LET-653(ZPc). If, as previously proposed [35], cleavage relieves an inhibitory ZPn-ZPc interaction, then cleavage should no longer be required when the ZPn is absent. In contrast, if cleavage changes ZPc conformation to enable ZPc interactions, then cleavage should still be required in the absence of ZPn. LET-653(ZPc, AYAA) localized efficiently to the apical membrane of the vulva and to the duct lumen of embryos, and partially
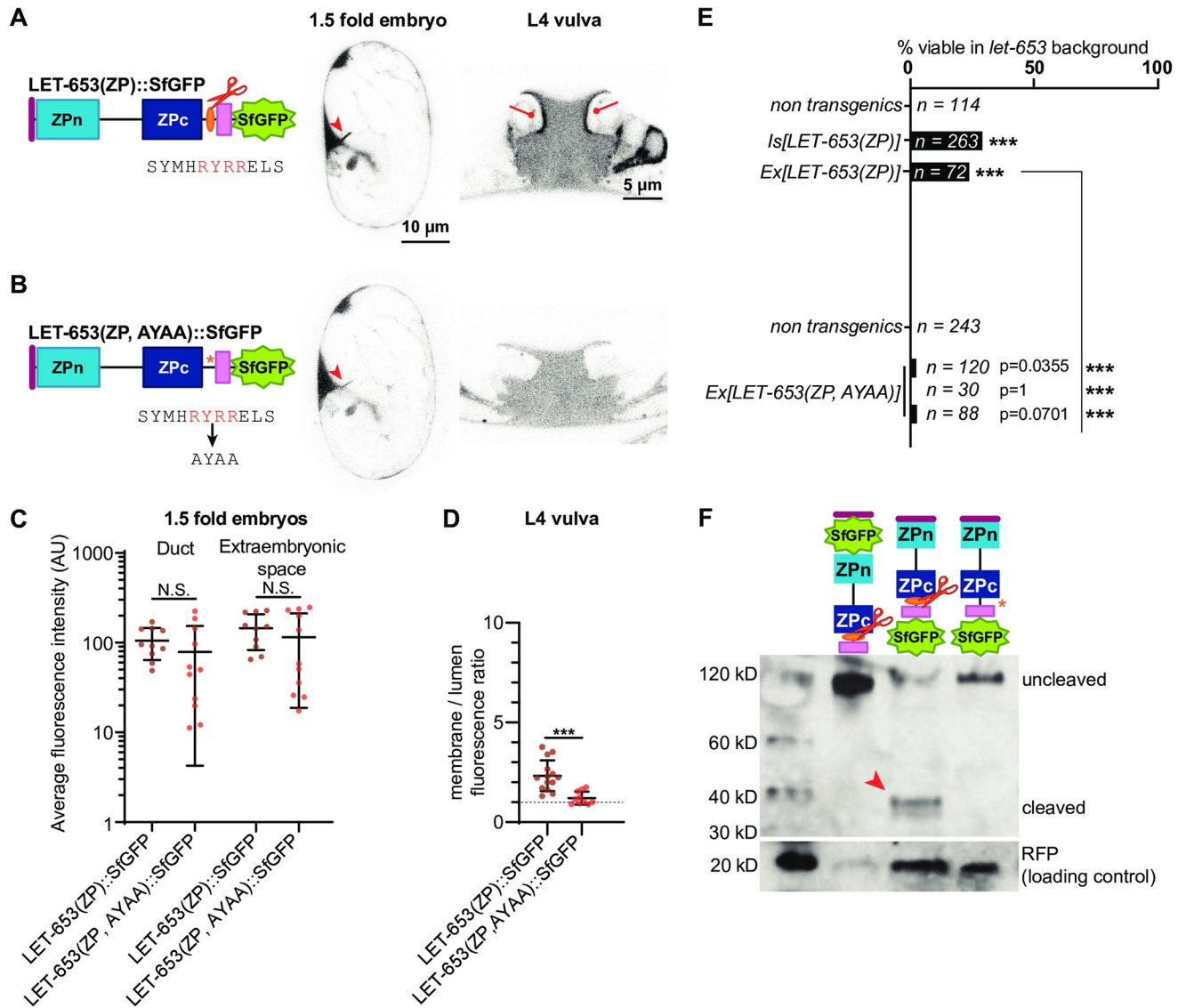
Fig 4. Cleavage promotes function and localization of the LET-653 ZP domain. A) LET-653(ZP)::SfGFP localized consistently to the embryonic duct lumen and the larval vulva dorsal apical membranes. B) LET-653(ZP, AYAA) cleavage mutant. The conserved CCS (red) was mutated to AYAA. Although LET-653(ZP, AYAA) was sometimes found in the embryonic duct lumen, it was never observed at vulva apical membranes. C) Duct and extraembryonic fluorescence in 1.5 fold embryos (see Fig 1). p>0.01, Mann Whitney two-tailed U test. Error bars; standard error. D) Ratio of apical membrane-associated to lumen fluorescence in the L4 vulva (see Fig 1). ***p<0.0001, Mann Whitney two-tailed U test. Dashed line indicates a ratio of 1, where membrane fluorescence is equal to luminal fluorescence. Error bars; standard error. E) LET-653(ZP)::SfGFP was partly functional in a *let-653* mutant background, though rescue was not as strong as that seen with N-terminally tagged transgenes (compare to Fig 2F). Three independent lines of LET-653(ZP, AYAA):: SfGFP had little activity. Although the comparisons to non-transgenic siblings are not statistically significant, the few survivors likely represent some biological function for LET-653(ZP, AYAA), as *let-653* mutants never survive [52]. ***p<0.001, two-tailed Fisher's Exact test. F) Western blot demonstrating abrogation of cleavage. SfGFP::LET-653(ZP) runs at ~120 kD while LET-653(ZP)::SfGFP runs at ~40 kD, indicating that LET-653 is cleaved at its C-terminus as previously reported [52]. LET-653(ZP, AYAA)::SfGFP runs at nearly the same size as N-terminally tagged LET-653, indicating it is not cleaved. Loading control is RFP, which is co-expressed from transgenes containing LET-653 and whose expression is proportional to the amount of LET-653 in transgenic *C. elegans*. Blot is representative of n = 4 biological replicates.

rescued *let-653* mutant duct defects (Fig 5B, 5C–5E). Western blots confirmed that LET-653 (ZPc, AYAA) was rarely cleaved (Fig 5F). We conclude that cleavage is not required for localization of the isolated ZPc domain but does promote its function. These results suggest that LET-653(ZPc) can bind to a relevant matrix partner without being cleaved, but that cleavage
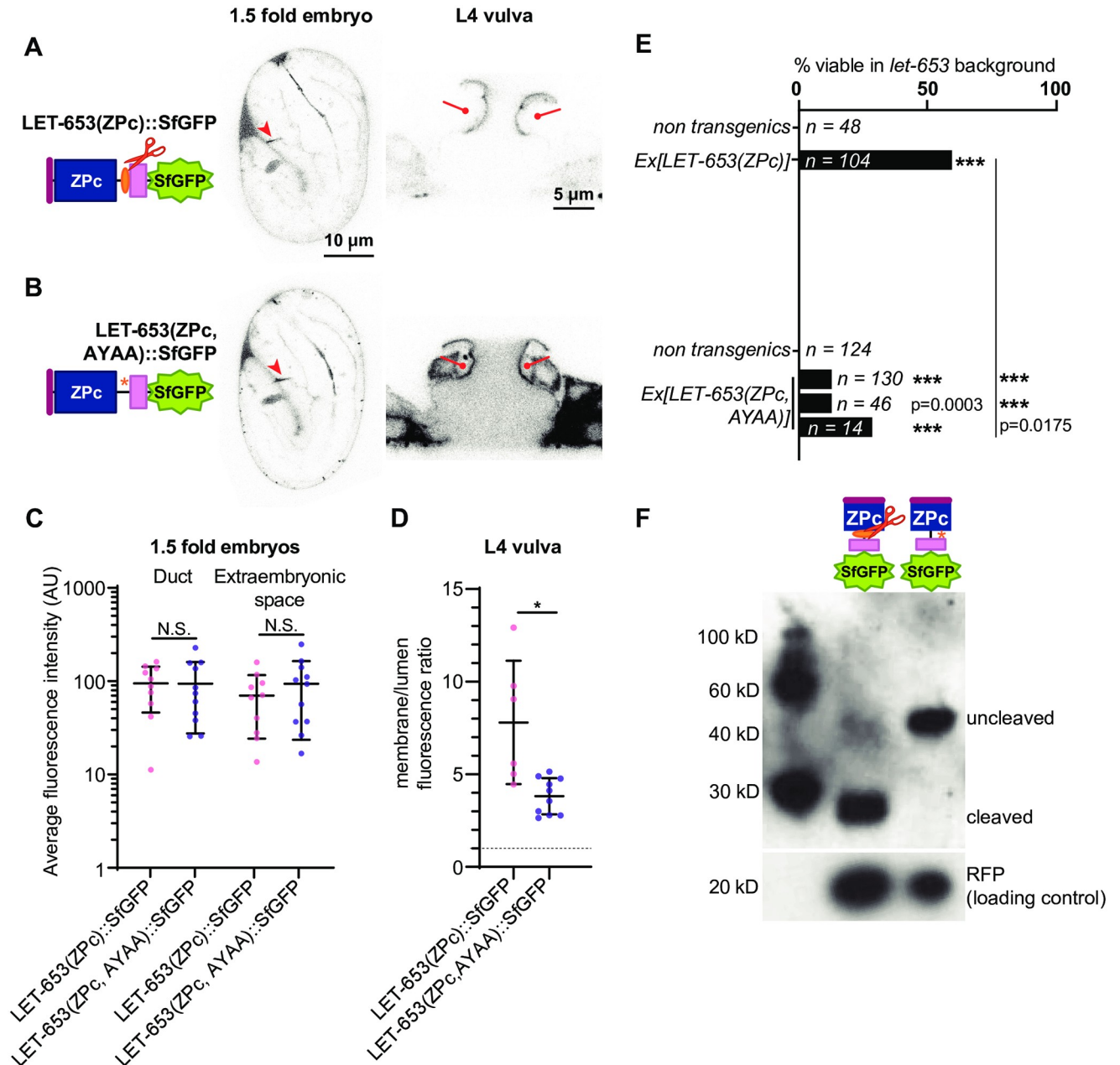
Fig 5. LET-653 cleavage relieves ZPn-dependent inhibition of ZPc localization and promotes ZPc function. A) LET-653(ZPc)::SfGFP and B) LET-653 (ZPc, AYAA)::SfGFP both localized to the duct lumen and vulva apical membranes. C) Duct and extraembryonic fluorescence in 1.5 fold embryos within boxes drawn on relevant structures (see S1 Fig). p>0.01, Mann Whitney two-tailed U test. Error bars; standard error. D) Ratio of membrane-associated to lumen fluorescence in the L4 vulva (see S1 Fig). *p = 0.0047, Mann Whitney two-tailed U test. Dashed line indicates a ratio of 1, where membrane fluorescence is equal to luminal fluorescence. Error bars; standard error. E) LET-653(ZPc)::SfGFP rescued *let-653* mutants. Despite localizing normally, 3/3 lines of LET-653(ZPc, AYAA)::SfGFP only partially rescued *let-653* mutants. ***p<0.001, two-tailed Fisher's Exact test. F) Western blot demonstrating abrogation of cleavage. LET-653(ZPc)::SfGFP runs at ~40 kD. Mutating the cleavage site (see Fig 4A) resulted in a protein that ran at ~60kD, close to the estimated size of the entire protein fragment based on amino acid sequence. Loading control is RFP (see Fig 4). Blot is representative of n = 3 biological replicates.

https://doi.org/10.1371/journal.pgen.1009188.g005

may release inhibition of this binding by the ZPn domain. Cleavage also changes other functional properties of the LET-653(ZPc) module and/or releases the C-terminus for function.

LET-653(ZPc) incorporates stably into the aECM

To test if LET-653(ZPc) incorporates stably into the aECM, we performed FRAP analysis. In line with previous results [52], roughly 50% of LET-653(ZP) fluorescence was bleached and this fluorescence showed incomplete recovery, indicating that at least some of LET-653(ZP) is immobile in its aECM layer (Fig 6A, S3 Fig). In contrast, bleaching of secreted SfGFP was difficult to detect, likely due to swift recovery and replacement of SfGFP molecules from other parts of the vulva lumen (S3 Fig). A limited amount of LET-653(ZPc) fluorescence could be effectively bleached, though similar to LET-653(ZP), the bleached portion showed limited recovery (Fig 6B–6E, S3 Fig). Resistance to bleaching could indicate that 1) a portion of LET-653(ZPc) is highly mobile, similar to SfGFP alone, and recovers before bleaching can be detected; or 2) LET-653(ZPc) integrates into an aECM structure that shields the fluorescent protein from bleaching. In any case, incomplete recovery of the bleached portion of LET-653 (ZPc) is consistent with a portion of the protein stably incorporating into an aECM layer.

The LET-653 ZPc domain binds aggregates *in vitro*

To test whether the LET-653 ZPc domain polymerizes or aggregates, we expressed tagged LET-653 fragments in *Drosophila* S2R+ cells. LET-653(ZP) or LET-653(ZPc) were efficiently secreted and properly cleaved by S2R+ cells, as assessed by Western blotting (S4 Fig). As previously observed, another *C. elegans* ZP protein, DYF-7, formed large fibrils on the surface of S2R+ cells [54], but LET-653 fragments formed no such structures and instead appeared diffuse (S4 Fig). However, using higher magnification, we observed large crystalline aggregates throughout the cell media (Fig 7). Aggregates were present but not fluorescent in media from S2R+ cells transfected with empty vector (EV), SfGFP, or the LET-653(ZPn) domain (Fig 7A, 7B, 7D and 7H). In contrast, aggregates were fluorescent in media containing LET-653(ZP) or LET-653(ZPc) (Fig 7C, 7E, 7F and 7H). Media containing LET-653(ZP, AYAA) had crystalline aggregates that were similar in brightness to those of media containing LET-653(ZP) (Fig 7F–7H). The number of aggregates varied between technical replicates and did not correlate with genotype (S5 Fig). We conclude that the aggregates consist primarily of components derived from S2R+ cells or media, and that LET-653 binds these aggregates but does not stimulate their formation. Furthermore, efficient aggregate binding *in vitro* correlates well with efficient matrix incorporation and function *in vivo*.

To test the properties of the observed aggregates, we examined whether they stained with amyloid dyes or were heat sensitive. The dye Nile Red stained aggregates whether secreted LET-653(ZPc) was present or not (Fig 8). This dye binds amyloid structures, as well as hydrophobic materials and some salt crystals [65–67]. To test heat sensitivity, we heated freshly thawed media to 50˚C for fifteen minutes. Imaging revealed that fluorescent aggregates remained after heating (Fig 8C). The fact that these aggregates can be labeled with dyes and are non-heat-soluble indicates that they may have some biochemical characteristics of amyloid. Future studies are needed to determine the composition of these aggregates and any relationship they might have to the endogenous matrix partners of LET-653 *in vivo*.

Discussion

Although ZP proteins are critical components of aECMs in metazoans, how ZP proteins assemble in aECMs remains poorly understood. In this study, we investigated how one *C. elegans* ZP protein, LET-653, assembles into aECMs. We found that, counter to prevailing models
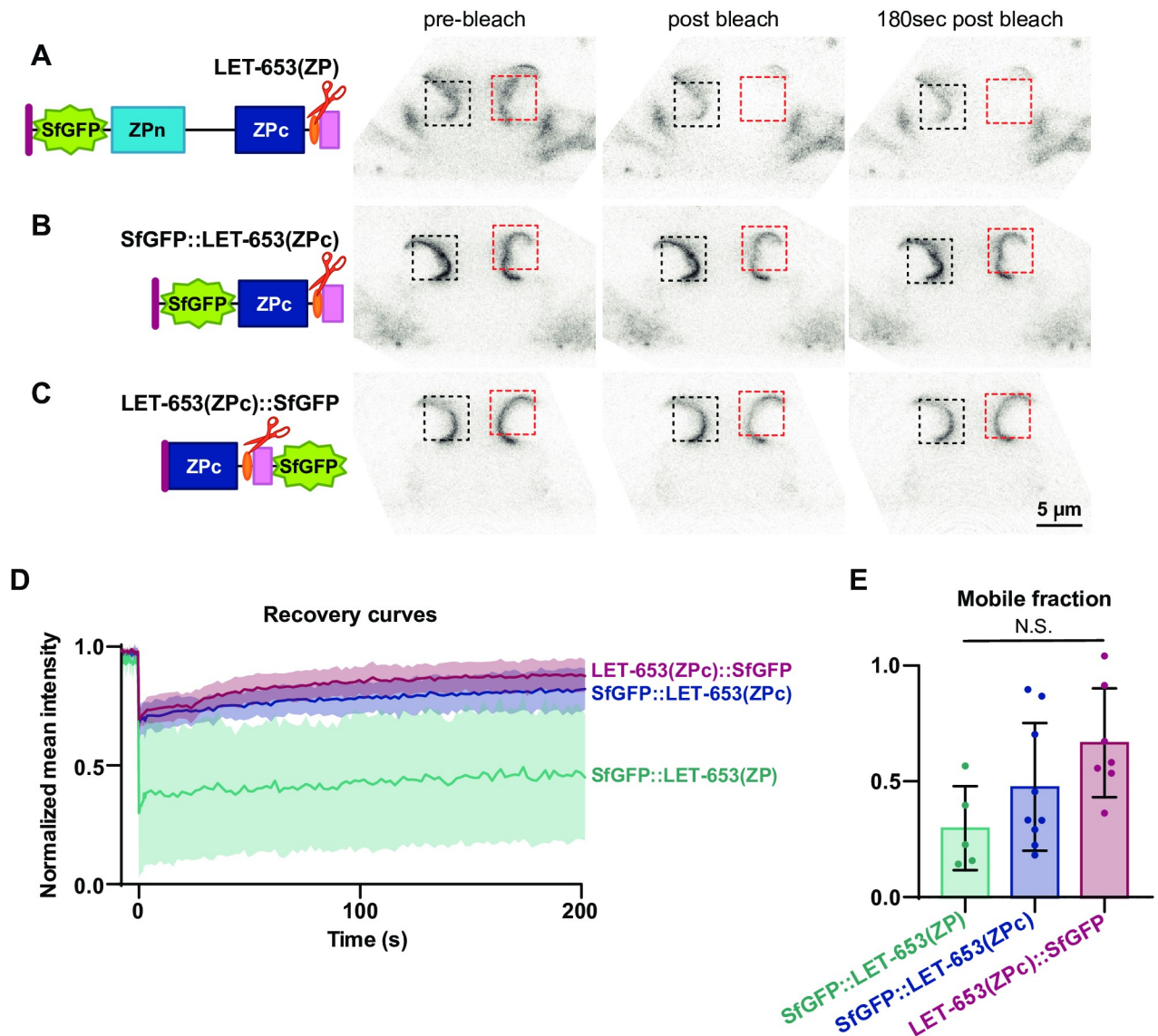
Fig 6. A portion of LET-653(ZPc) is immobile in the vulva aECM. Fluorescence recovery after photobleaching (FRAP) of LET-653 translational fusions in the vulva lumen. Pre-bleach, bleach, and post-bleach frames taken from FRAP experiment on mid-L4 vulvas. Red box; bleached region of interest. Black box; unbleached region of interest. Background regions of interest are outside the field of view. A) FRAP of SfGFP::LET-653(ZP) (*csEx624*). LET-653(ZP) is bleached but then recovers poorly. Representative of n = 4 replicates. B) FRAP of SfGFP::LET-653(ZPc) (*csEx821*). Representative of n = 8 replicates. C) FRAP of LET-653(ZPc)::SfGFP (*csEx841*). Representative of n = 7 replicates. LET-653(ZPc) was not efficiently bleached regardless of the location of the SfGFP tag. D) Fluorescence recovery curves with mean and standard error for each LET-653 fusion protein. t = 0s represents the first post-bleach frame. E) Mobile fraction calculated from recovery curves. No significant difference was measured between any groups (two tailed Mann-Whitney U test), though poor bleach efficiency could reflect a pool of highly mobile LET-653(ZPc). Error bars; standard error.

https://doi.org/10.1371/journal.pgen.1009188.g006

for ZP assembly, LET-653 functions and localizes via its ZPc domain (Fig 9A and 9B). Cleavage of the C-terminus may release inhibition of the ZPc by the ZPn domain, but also promotes ZPc function via some other mechanism. *In vitro*, LET-653(ZPc) spontaneously incorporates into large aggregates. These data demonstrate that ZPc domains can function independently to assemble in aECMs, functions that were previously attributed only to ZPn domains.
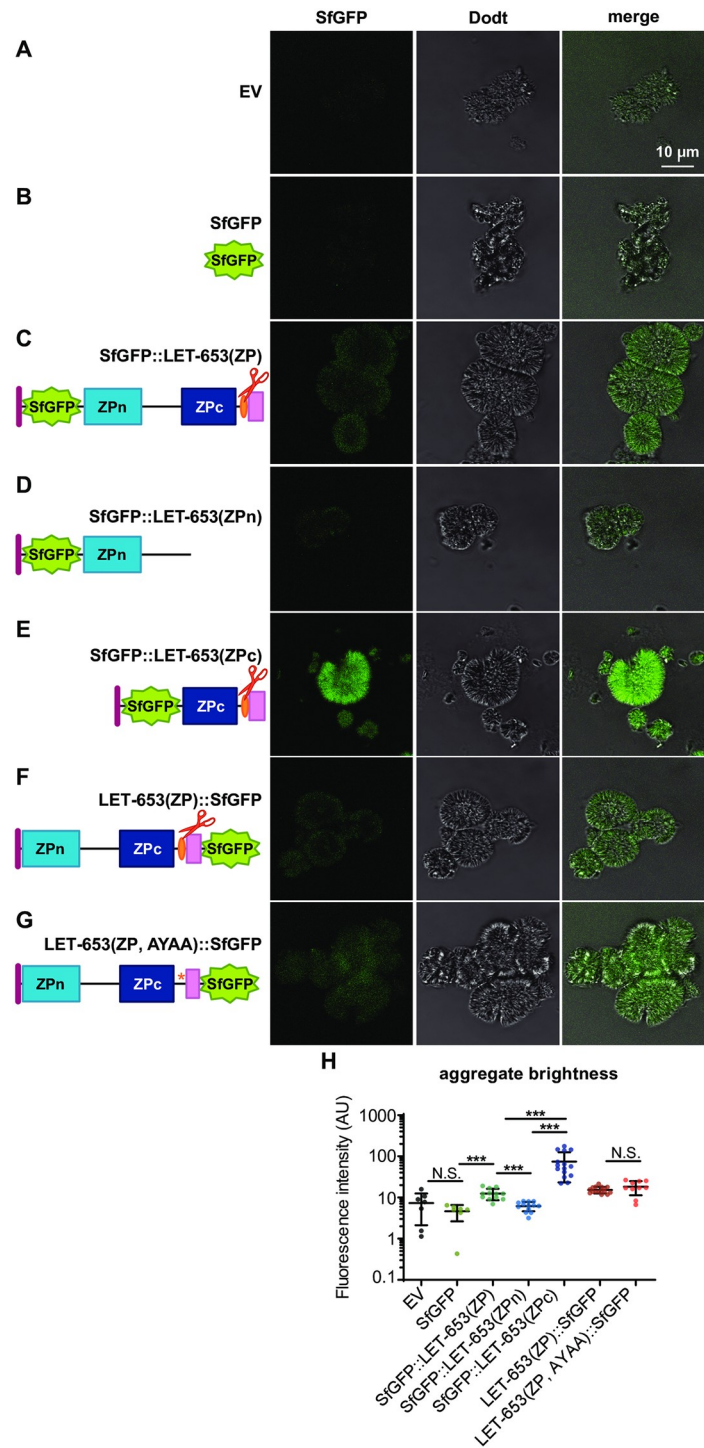
Fig 7. The LET-653 ZPc domain binds aggregates *in vitro*. A-G) Single confocal slices of freshly thawed cell media. A-B) Aggregates were non-fluorescent in EV- or SfGFP- transfected cell media. C) Aggregates were fluorescent in SfGFP::LET-653(ZP)-transfected media. D) SfGFP::LET-653(ZPn)-transfected media resembled negative controls; E) SfGFP::LET-653(ZPc) transfected cell media contained aggregates of high fluorescence intensity. F-G) Aggregates in media containing LET-653(ZP)::SfGFP and LET-653(ZP, AYAA)::SfGFP were similarly fluorescent. H) Quantification of aggregate fluorescence intensity. ***p<0.0001; two-tailed Mann-Whitney U test. Error bars; standard error. All experiments were performed on media from transfection 2.

https://doi.org/10.1371/journal.pgen.1009188.g007

Fig 8. LET-653-bound aggregates stain with dyes and are not heat-labile. A-B) Aggregates stained with the lipid dye Nile Red regardless of whether LET-653(ZPc) was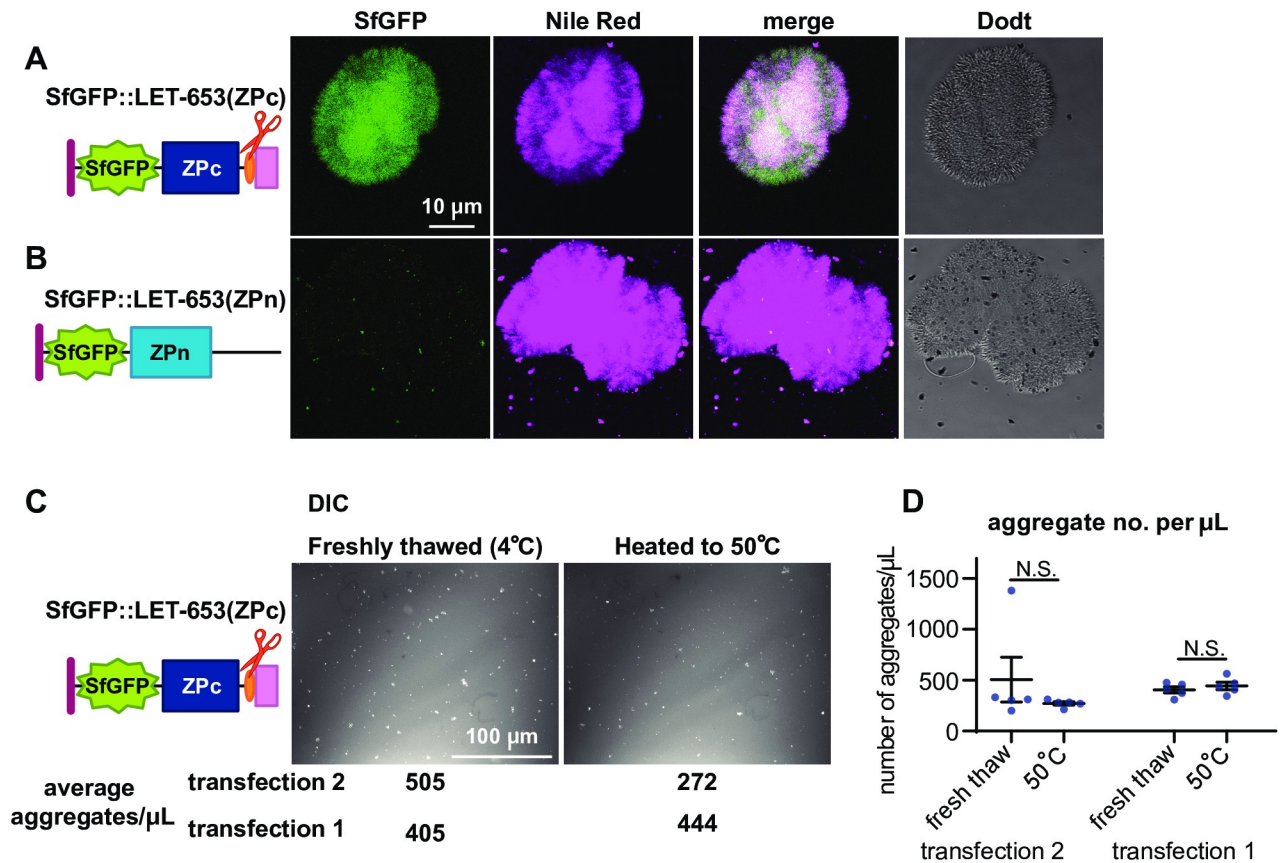 present. A) LET-653(ZPc) and Nile Red co-labelled aggregates. B) When LET-653(ZPc) was absent, aggregates, which were rare, still stained strongly with Nile Red. C) DIC images of LET-653(ZPc) aggregates. Aggregates were plentiful in freshly thawed media and remained after media was incubated for 15 minutes at 50 ˚C. D) Quantification of aggregate number. No significant differences were seen between any groups, two-tailed Mann Whitney U test. Error bars; standard error.

https://doi.org/10.1371/journal.pgen.1009188.g008

ZPc domains can function independently of ZPn domains

ZPc domains have been generally assumed to support ZPn domains and not to function independently [30]. Initial surveys of ZP proteins across phyla suggested that some contain ZPn domains without ZPc domains, and yet are still capable of polymerization [36], while proteins with only ZPc domains were not thought to exist [30]. However, we and others found that *C. elegans* does have five predicted ZPc-only proteins [34, 68]. In proteins like uromodulin that have polymerizing ZPn domains, ZPc domains are thought to inhibit the ZPn domain [30]. While our study was under review, two groups reported cryo-EM structures for full-length uromodulin that suggest filament assembly involves interactions of both ZPn and ZPc domains with linker regions of other monomers, which would suggest that both domains are functionally important [69, 70]. In the TGFβ receptors Betaglycan and Endoglin, ZPc domains dimerize and can bind ligands, but have not been reported to form higher-order structures [28, 29, 71]. Our results indicate that ZPc domains can function independently of ZPn domains for both matrix incorporation and tissue-shaping.

In fact, in the case of LET-653, the ZPn domain inhibits ZPc activity, perhaps to confine ZPc activity to precise times and places within the aECM. We did not detect any independent
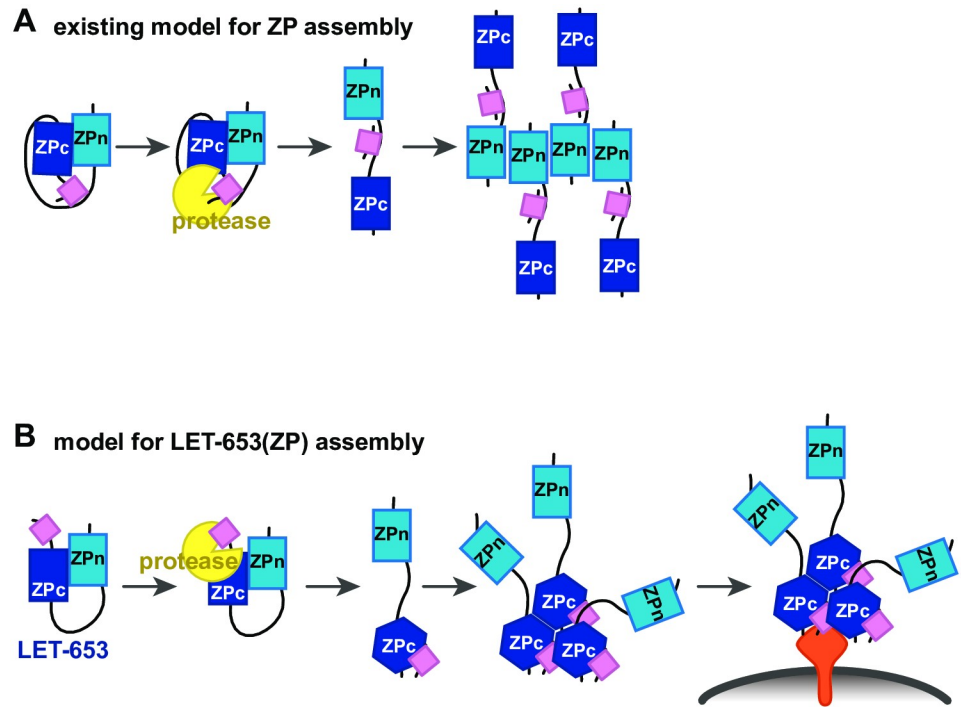
Fig 9. Model for LET-653 matrix assembly. A) Traditional model for ZP assembly. Prior to cleavage, the hydrophobic C-terminus (pink box) interacts with a hydrophobic patch in the linker (black line). This interaction causes the ZPc domain to inhibit the ZPn domain from interacting with itself or other partners. After the C-terminus is cleaved by a protease (yellow), the ZPn domain is free of inhibition and polymerizes. B) Model for LET-653 assembly. Prior to cleavage, the ZPn domain inhibits the ZPc domain. After cleavage, the C-terminus (pink box) associates with the ZPc domain, which changes conformation. The ZPn domain no longer inhibits the ZPc domain. The ZPc domain oligomerizes and binds a membrane-anchored partner(s) (orange). Membrane; gray line.

role for the ZPn domain in shaping the duct lumen, and this domain is not able to localize specifically in the vulva aECM. This result is surprising given the centrality of ZPn domains to most models of ZP function [30]. The LET-653 ZPn domain lacks a key tyrosine residue present in most polymerizing ZP proteins [41, 52], which could explain functional differences between the LET-653 ZPn domain and others. Intriguingly, this tyrosine residue is also absent in a number of other *C. elegans* ZP proteins [61], the *Drosophila* protein Zye [50] and some mammalian proteins including Endoglin [41] and Oit3 (S6 Fig). Researching additional ZP proteins may reveal that both ZPn and ZPc domains can have diverse functions, and that either domain, or both domains simultaneously, can direct matrix incorporation.

The LET-653 ZPc domain has additional cysteines compared to some ZP proteins. ZPc domains fall into several families, with 4, 6, or 8 cysteines [30, 34]. The LET-653 ZPc domain has 8, as does the Zona Pellucida ZP protein ZP3 [30,33]. Like LET-653, ZP3 has a cleaved C-terminus that can bind the ZPc domain [33]. It is possible that all ZPc domains with 8 cysteines have analogous assembly mechanisms. Testing the assembly of additional proteins in this class may expose patterns in ZP structure and function.

Cleavage promotes two separable aspects of ZPc function

Intramolecular interactions between ZPn and ZPc domains during cellular trafficking are thought to hold ZP proteins in an inactive conformation to prevent premature

oligomerization [30]. C-terminal cleavage, perhaps by proteases at the plasma membrane, relieves this auto-inhibition to allow matrix incorporation [43, 45, 48]. Our data are consistent with this model, although the relative roles of the ZPn vs ZPc domains are reversed. Our data further suggest that cleavage promotes two distinct roles of the ZPc domain: 1) the ability to bind to a matrix partner that determines spatial specificity; and 2) some other change that is essential for tube-shaping function. Cleavage may relieve ZPn-dependent inhibition of the first role, but the second role still requires cleavage even in the absence of the ZPn domain.

The relevant matrix partner(s) of LET-653(ZPc) are not known, but they appear to be located on the apical surfaces of the excretory duct tube and vulE and vulF vulva cells. Although *let-653* is expressed by all vulva cells [52], genetic perturbations to increase or eliminate vulE or vulF cell types showed that these cells have a specific ability to recruit LET-653 (ZP) [61]. Furthermore, vulF cells contain large matrix-secreting vesicles whose contents appear disorganized in *let-653* mutants, suggesting that LET-653 may traffic through the same compartment with its partner(s) [61]. Identifying the relevant partner(s) may require a combination of genetic and biochemical approaches and would likely offer crucial insight into how LET-653 incorporates into matrix and shapes tubes.

The second ZPc function enabled by cleavage might be oligomerization, binding to a second partner, and/or release of the hydrophobic C-terminus for function. A portion of LET-653(ZPc) appears immobile in the aECM *in vivo* (Fig 6) and incorporates into crystalline aggregates *in vitro* (Fig 7), consistent with the possibility that LET-653(ZPc) may oligomerize to form its matrix layer *in vivo*. Our data further indicate that the cleaved C-terminus stays associated with the ZPc domain, since LET-653(ZPc) tagged at either end results in identical localization patterns. Models for ZP organization generally show the C-terminus binding to the linker [35], but the crystal structure of the protein ZP3 indicates the C-terminus can bind the ZPc domain [41]. Furthermore, the C-terminus alone can confer aggregation properties when attached to the ZPn domain (Fig 3). We propose that a cleavage-dependent change in the relative conformations of the main ZPc and C-terminus may facilitate oligomerization and interactions with other partners (Fig 9B).

LET-653 incorporates into roughly spherical aggregates that resemble salt crystals. These aggregates may consist largely of protein or could represent protein-salt complexes. Intriguingly, salt appears to stimulate uromodulin to form filaments [35]. Furthermore, the ZP protein Oit3 (also known as LZP), a proposed partner of uromodulin, can form spherical aggregates of unknown organization *in vitro* [31]. However, how these Oit3 aggregates assemble, if they include other co-factors, such as uromodulin or salts, and whether they form *in vivo* is not clear. Previous *in vitro* studies of ZP proteins have been challenging, as many cell types fail to cleave or secrete intact ZP proteins appropriately [33, 35]. S2R+ cells fortuitously express a compatible protease and offer a straightforward model to assess ZP assembly and to characterize ZP-containing aggregates.

Conclusion

ZP proteins are a diverse family of aECM components that are found across the animal kingdom. ZP proteins shape many apical surfaces [14], changes in ZP protein expression or structure are implicated in the evolution of morphological features [72] and speciation [73], and ZP protein loss contributes to multiple human diseases. This work harnessed *C. elegans* to demonstrate a new mode of ZP protein assembly in which the ZPc domain is the primary functional unit. Future work should take advantage of additional tractable models to characterize the true diversity of ZP protein function and assembly mechanisms.

Materials and methods

Worm strains, alleles and transgenes

All strains were derived from Bristol N2 and were grown at 20°C under standard conditions [74]. *let-653* mutants were obtained from mothers rescued with a *let-653*(+) transgene [52]. Mutants used were *let-653(cs178)* (an early nonsense allele) [52]. Strain generated using CRISPR/Cas9 was *let-653(cs262[LET-653::SfGFP])* [61]. See S1 Table for a complete list of strains generated in this study.

Staging and microscopy

Embryos were selected at the 1.5-fold stage based on morphology. Larvae were staged by size and vulva lumen morphology. Fluorescent, brightfield, Differential Interference Contrast (DIC), and Dodt (an imaging technique that simulates DIC) [75] images were captured on a Zeiss Axioskop compound microscope fitted with a Leica DFC360 FX camera or with a Leica TCS SP8 confocal microscope (Leica, Wetzlar Germany). Images were processed and merged using ImageJ.

Quantification of LET-653 fluorescence

To confirm that LET-653 transgenes were adequately expressed, their fluorescence intensity was measured in embryos within boxes drawn on single confocal slices. Boxes were drawn either to fit the small duct lumen using the ImageJ "Rotated rectangle" tool or were drawn to roughly 3x3 microns within the extraembryonic space (Fig 1D). The average fluorescence intensity per pixel within those regions was measured using the ImageJ "Mean gray value" tool.

Measurements of LET-653 enrichment at the vulva vulE and vulF cell apical membranes were performed as in Bidaud-Meynard et al. [76]. 10 pixel-thick-lines were drawn across the dorsal region of the vulva, including both apical membranes. 5 pixel values representing LET-653 fluorescence intensity at each apical membrane (totaling 10 values) were averaged and divided by 10 pixel values from the luminal region directly between the vulE and vulF apical membranes (Fig 1G). All measurements are taken from single confocal Z-slices. Final values reported are ratios.

let-653 transgenes

All *let-653* transgenes were generated by inserting LET-653 fragments into the plasmid pJAF5, which contains a 2.2 kb fragment containing the *let-653* promoter and upstream regulatory region [52]. All plasmids were generated via restriction enzyme cloning and were verified by Sanger sequencing. *let-653* encodes three isoforms of a protein with two N-terminal PAN/Apple domains and a ZP domain. As the shortest isoform, LET-653b, was previously shown to be sufficient for function, all structure-function constructs are based on LET-653b (GenBank accession no: X91045.1) [52]. Plasmids were co-injected at concentration 17 ng/μL with marker pHS4 (*lin-48pro*::mRFP) at concentration 50 ng/μL. Integrated transgenes were generated using TMP/UV as described [77] and include: *csIs92 [let-653pro::SfGFP::LET-653(ZPc); lin-48pro::mRFP]*, *csIs95 [let-653pro::LET-653(ZP, AYAA)::SfGFP; lin-48pro::mRFP]*, *csIs96 [let-653pro::LET-653(ZP)::SfGFP; lin-48pro::mRFP]*. In most cases, two or three independent lines of each transgene were assayed for rescue activity and gave similar results. Only a single line per transgene was used for the image quantifications shown. A complete list of transgenes, primers, and plasmids generated for this study can be found in S2 Table.

FRAP

Specimens were mounted on 10% agarose pads containing 20 mM sodium azide and 10 mM levamisole in M9 after Gill et al., 2016 [52]. FRAP was performed using Leica Application Suite X software FRAP module on a Leica TCS SP8 MP confocal microscope. Three regions of interest of 3×3 μm were defined within the wizard: a bleached region of interest (bleached ROI), an unbleached ROI of similar fluorescence intensity, and a background ROI drawn in a region that did not include an animal. Maximum laser intensity was used for bleaching experiments and experiments were carried out over the course of a single imaging session. Mean fluorescence intensities within the ROIs were measured at specified intervals. Background ROI values were subtracted from both the bleached and unbleached ROI values. Corrected bleach ROI values then were divided by corrected unbleached ROI values (bleached—background / unbleached—background), and the resulting ratios were normalized such that the maximum intensity was set to 1. The following experimental time-course was used: 20 prebleach frames every 0.4 sec, 10 bleach frames every 0.4 sec, and 90 postbleach frames every 2.0 sec. Pre- and postbleach laser intensity was set to 1% and bleach laser intensity was set to 100%. FRAP plots were created using Prism (Graphpad, San Diego California). Mobile fraction = (recovery fluorescence—postbleach fluorescence) / (prebleach fluorescence—postbleach fluorescence) [78].

FRAP shown in Fig 6 was performed on strains bearing extrachromosomal transgenes *csEx624 [let-653pro::SfGFP::LET-653(ZP); lin48pro::mRFP], csEx821 [let-653pro::SfGFP::LET-653(ZPc); lin-48pro::mRFP]*, and *csEx841 [let-653pro::LET-653(ZPc)::SfGFP; lin-48pro::mRFP]*. FRAP shown in S3 Fig was performed on strains bearing transgenes *csEx636 [let-653pro::ssSfGFP; lin48pro::mRFP], csIs66 [let-653pro::LET-653(ZP)::SfGFP; let-653pro::PH::mCherry] X*, and *csIs92 [let-653pro::SfGFP::LET-653(ZPc); lin-48pro::mRFP]*. Expression levels from the integrated transgenes tended to be lower and less variable than those from extrachromosomal transgenes, but both gave similar overall results.

Drosophila cell culture and media experiments

S2R+ cells were cultured under standard conditions [79]. Cells were transfected using Effectene (Qiagen, 301427, Venlo Netherlands). Plasmids for transfection were generated by inserting cDNAs containing *let-653b* into pAC5.1 as XbaI—EcoRI fragments alongside the *unc-54* 3' UTR as an EcoRI—ApaI fragment. Three sets of S2R+ cells were independently transfected with 1 μg DNA of the indicated constructs. Cells were grown under standard conditions for 72 hours before imaging and media collection. Cells were imaged under brightfield and fluorescence microscopy using a Leica SP5 confocal microscope, and media and cells were then collected for further analysis. Media was collected by pipetting and was then centrifuged for 1 min at 10,000. Cells were washed in PBS then lysed via incubation for 20 minutes at 4 ˚C in 1 ml lysis buffer (50 mM Tris-HCl pH 7.4, 500 mM NaCl, 1% NP40, 1 mM EDTA, 0.25% sodium deoxycholate, 1 mM sodium orthovanadate, 1× complete protease inhibitor cocktail (Roche, Basel Switzerland) and 1 mM PMSF). Cell lysates were centrifuged for 20 minutes at 4 ˚C at 10,000 rpm to remove debris. Media and cell lysates were stored at -80 ˚C until ready for use. All three sets of transfections showed evidence of LET-653 secretion and cleavage as assessed by Western blotting. Two out of two tested sets of transfections showed evidence of ZPc binding to aggregates.

To image aggregates, 3 μL freshly thawed media was pipetted onto glass slides. DIC images for counting aggregates were obtained with a Zeiss Axioskop. 5 evenly spaced 92 mm x 92 mm fields of view were imaged per slide. To quantify aggregate number, DIC images were first subjected to a grayscale threshold filter in ImageJ (default threshold; limits: 85–255) and then aggregates were counted using the 3D Particle Counter plugin. The number of aggregates per

field of view was adjusted to represent the number of aggregates per μL. To measure fluorescence intensity of aggregates, a box of 5 x 5 microns was drawn within aggregates and the average intensity per pixel (Mean gray value) was recorded from a single confocal Z-slice. A minimum of 5 aggregates per sample were measured.

To measure aggregate stability at different temperatures, 12 μL of media was thawed and aliquoted. 3 μL of this media was immediately pipetted onto glass slides for imaging. The remaining 12 μL of media was heated to 50˚C in a thermocycler for 15 minutes and then a portion was immediately imaged. Another portion was reserved and cooled to 4˚C in a thermocycler for 15 minutes before imaging. Aggregate number from DIC images was quantified as described above, except that before thresholding, images were processed using the ImageJ plugin "Background Correction". To stain aggregates with Nile Red, a solution of 100 mM in acetone was mixed with media for a final concentration of 1 mM and the sample was then imaged immediately.

Western blotting was performed on 5 μL of media or cell lysate as described below.

Western blotting

Early embryos were collected via the alkaline bleach method [80] from two 60 mm plates of nearly confluent worms and embryos were allowed to develop in M9 for 4–5 hours until they reached 1.5-fold stage. Worms were pelleted and transferred to Laemmli buffer (Bio-Rad, 161–0737) with 1x Protease Inhibitor Cocktail (Sigma, 2714) and 1:20 β-mercaptoethanol. Samples were transferred to -80C until ready for use. Samples were boiled for 10 minutes and then loaded into Mini-Protean TGX gradient gel (Bio-Rad, 456–1084) or a 15% acrylamide gel. Electrophoresis was performed at 0.02–0.03A under 1x electrophoresis buffer (Bio-Rad, 161–0732). Protein was transferred onto 0.2um nitrocellulose membrane (Bio-Rad, 162–0147) overnight in 1x transfer buffer (20% ethanol, 0.58% Tris Base, 2.9% Glycine, 0.01% SDS). Membranes were washed in PBS + 0.02% Triton (PBST), blocked for 1 hour at room temperature in PBST + 10% dry, nonfat milk, and then probed for GFP for 1 hour at room temperature with PBST + 10% milk + 1:1000 anti-GFP antibody (Rockland Immunochemicals, 600-101-215). To visualize the signal, Membranes were washed in PBST, probed with PBST + 10% milk + 1:5000 anti-Goat-HRP antibody (Rockland Immunochemicals, 605–4302) for 1 hour at room temperature and then washed with PBST before detection using SuperSignal West Femto Maximum Sensitivity Substrate (Pierce 34095) and film. Loading controls were carried out as described above using 1:1000 anti-RFP antibody (Abcam, ab62341) and 1:10,000 anti-rabbit-HRP antibody (GE Healthcare, NA934V). RFP corresponds to the *lin-48p::mRFP* co-injection marker present in all transgenes, and therefore reflects the number of transgenic animals present in each sample.

Supporting information

S1 Fig. Method of measuring LET-653 in embryos and vulva. A-A') Levels of LET-653 fluorescence in the 1.5 fold embryo. Functional transgenes were generally expressed at similar levels to endogenous LET-653 in the duct lumen, but accumulated to much higher levels in the extraembryonic space. Error bars; standard error. B) Quantification of membrane-associated vs. luminal LET-653 in the mid-L4 vulva for all groups. C-terminally and N-terminally tagged LET-653(ZP) and LET-653(ZPc) are not significantly different from one another. However, LET-653(ZPc, AYAA) is significantly more enriched at the apical membrane than LET-653 (ZP, AYAA), and this result correlates with increased function in LET-653(ZPc, AYAA) vs LET-653(ZP, AYAA) (Figs 4–5). Dashed line indicates a ratio of 1, where membrane fluorescence is equal to luminal fluorescence. Error bars; standard error.
(DOCX)

S2 Fig. LET-653(ZP, AYAA) is cleared normally from the embryonic duct. LET-653(ZP) and LET-653(ZP, AYAA) are both present in the duct lumen at 1.5 fold stage but are gradually cleared over several hours. Presence of LET-653 in the duct lumen was assessed visually via epifluorescence microscopy. LET-653(ZP, AYAA) was sometimes too faint to be detected within the duct lumen at the 1.5 fold stage. n = 20 for each time point.
(DOCX)

S3 Fig. LET-653(ZPc) and LET-653(ZP) show similarly limited mobility. Fluorescence recovery after photobleaching (FRAP) of LET-653 translational fusions in the vulva lumen. These experiments, which used integrated transgenes, gave similar results to those in Fig 6. Pre-bleach, bleach, and post-bleach frames taken from FRAP experiment on mid-L4 vulvas. Red box; bleached region of interest. Black box; unbleached region of interest. Background regions of interest are outside the field of view. A) FRAP of SfGFP (*csEx636*). Bleaching is not detected, possibly due to rapid replacement of bleached molecules by unbleached neighbors. Representative of n = 6 replicates. B) FRAP of SfGFP::LET-653(ZP) (*csIs66*). Representative of n = 6 replicates. C) FRAP of SfGFP::LET-653(ZPc) (*csIs92*). Representative of n = 6 replicates. D) Fluorescence recovery curves with mean and standard error for each LET-653 fusion protein. t = 0s represents the first post-bleach frame. The limited SfGFP bleaching meant that mobile fractions were often negative values and could not be reliably calculated. E) Mobile fraction calculated from recovery curves. No significant difference was detected between groups, Mann Whitney two-tailed U test.
(DOCX)

S4 Fig. LET-653 is cleaved when expressed from S2R+ cells. S2R+ cells were transfected with 1 μg DNA of the indicated constructs. A-F) Epifluorescent images of cells 72 hrs post-transfection, representative of >100 cells per condition. Large intracellular or cell-bound fibrils (arrows) were visible from SfGFP::DYF-7 [54] (B), but not from SfGFP alone or any LET-653 protein fusion. Black bar; transmembrane domain. Purple boxes; DYF-7 ZP domain. G) Western blot of S2R+ cell lysate probed with anti-GFP. Both un-cleaved and cleaved versions (arrowheads) of LET-653(ZP) and LET-653(ZPc) were visible. H) Western blot of S2R+ cell media probed with anti-GFP. LET-653(ZP) and LET-653(ZPc) were efficiently cleaved and cleavage products were visible in the media (arrowheads). LET-653(ZP, AYAA) was not cleaved but was still secreted into the media. EV; Empty vector. Western blot of media is representative of three blots from the three independent transfection experiments. Western blot of cell lysates was performed using cells from transfection 2. All images shown are of cells or media from transfection 2.
(DOCX)

S5 Fig. Aggregate number does not correlate with LET-653 function. Quantification of aggregate density in media thawed and mounted on glass slides. A) Aggregate density in media from transfection 2, shown in Fig 7. *p = 0.0079, two-tailed Mann Whitney U test. B) Aggregate density in media from transfection 1. Aggregate number was high across all genotypes. LET-653(ZP,AYAA) had significantly more aggregates than the other groups. *p = 0.0079, two-tailed Mann Whitney U test. Error bars; standard error.
(DOCX)

S6 Fig. The human ZP proteins Oit3 and DMBT1 lack key tyrosine residues. Alignment of ZPn domains based on Monne et al., 2008[41] and Gill et al., 2016 [52]. Grey shading corresponds to known beta-strands in ZP3, blue indicates conserved cysteines and yellow indicates conserved aromatic residues. Like LET-653, Oit3 lacks the conserved aromatic residue in the F strand between Cys3 and Cys4, and DMBT1 lacks the second conserved aromatic residue after

Cys4. These two residues interact in the ZP3-N crystal structure [41] and are thought to be critical for ZPn polymerization. Genbank accession numbers: Ce_LET-653b: NP_001021337; Ce_DYF-7: NP_509630; Dm_Dpy: NP_001245875; Hs_UMOD: NP_003352; Hs_TectA: NP_005413; Hs_ZP3: NP_001103824; Hs_DMBT1: NP_004397; Hs_Oit3: NP_689848; Hs_Eng: NP_001108225.
(DOCX)

S1 Table. Strains generated in this study. All strains used or generated in this study are listed with full genotypes.
(DOCX)

S2 Table. Plasmids generated in this study. All plasmids generated in this study are listed with their contents and mechanism of assembly.
(DOCX)

Acknowledgments

Author Contributions

Conceptualization: Jennifer D. Cohen, Matthew C. Good, Meera V. Sundaram.

Data curation: Jennifer D. Cohen.

Formal analysis: Jennifer D. Cohen, Meera V. Sundaram.

Funding acquisition: Meera V. Sundaram.

Investigation: Jennifer D. Cohen, Jessica G. Bermudez.

Supervision: Matthew C. Good, Meera V. Sundaram.

Writing – original draft: Jennifer D. Cohen, Meera V. Sundaram.

Writing – review & editing: Jessica G. Bermudez, Matthew C. Good.

References

1. Luschnig S, Uv A. Luminal matrices: an inside view on organ morphogenesis. Exp Cell Res. 2014; 321 (1):64–70. https://doi.org/10.1016/j.yexcr.2013.09.010 PMID: 24075963

2. Gaudette S, Hughes D, Boller M. The endothelial glycocalyx: Structure and function in health and critical illness. J Vet Emerg Crit Care (San Antonio). 2020. https://doi.org/10.1111/vec.12925 PMID: 32067360

3. Halliday HL. The fascinating story of surfactant. J Paediatr Child Health. 2017; 53(4):327–332. https://doi.org/10.1111/jpc.13500 PMID: 28271629

4. Hansson GC. Mucus and mucins in diseases of the intestinal and respiratory tracts. J Intern Med. 2019; 285(5):479–490. https://doi.org/10.1111/joim.12910 PMID: 30963635

5. Gordts P, Esko JD. The heparan sulfate proteoglycan grip on hyperlipidemia and atherosclerosis. Matrix Biol. 2018; 71–72, 262–282. https://doi.org/10.1016/j.matbio.2018.05.010 PMID: 29803939

6. Husain N, Pellikka M, Hong H, Klimentova T, Choe KM, Clandinin TR, Tepass U. The agrin/perlecan-related protein eyes shut is essential for epithelial lumen formation in the Drosophila retina. Dev Cell. 2006; 11(4):483–493. https://doi.org/10.1016/j.devcel.2006.08.012 PMID: 17011488

7. Hwang HY, Olson SK, Esko JD, Horvitz HR. Caenorhabditis elegans early embryogenesis and vulval morphogenesis require chondroitin biosynthesis. Nature. 2003; 423(6938):439–443. https://doi.org/10.1038/nature01634 PMID: 12761549

8. Jovine L, Qi H, Williams Z, Litscher E, Wassarman PM. The ZP domain is a conserved module for polymerization of extracellular proteins. Nat Cell Biol. 2002; 4(6):457–461. https://doi.org/10.1038/ncb802 PMID: 12021773

9. Porter KR, Tamm I. Direct visualization of a mucoprotein component of urine. J Biol Chem. 1955; 212 (1):135–140. PMID: 13233216

10. Lane MC, Koehl MA, Wilt F, Keller R. A role for regulated secretion of apical extracellular matrix during epithelial invagination in the sea urchin. Development. 1993; 117(3), 1049–1060. PMID: 8325234

11. Syed ZA, Bougé AL, Byri S, Chavoshi TM, Tång E, Bouhin H, et al. A luminal glycoprotein drives dose-dependent diameter expansion of the Drosophila melanogaster hindgut tube. PLoS Genet. 2012; 8(8): e1002850. https://doi.org/10.1371/journal.pgen.1002850 PMID: 22876194

12. Chappell D, Jacob M, Paul O, Rehm M, Welsch U, Stoeckelhuber M. et al. The glycocalyx of the human umbilical vein endothelial cell: an impressive structure ex vivo but not in culture. Circ Res. 2009; 104 (11):1313–1317. https://doi.org/10.1161/CIRCRESAHA.108.187831 PMID: 19423849

13. Johansson ME, Sjovall H, Hansson GC. The gastrointestinal mucus system in health and disease. Nat Rev Gastroenterol Hepatol. 2013; 10(6):352–361. https://doi.org/10.1038/nrgastro.2013.35 PMID: 23478383

14. Plaza S, Chanut-Delalande H, Fernandes I, Wassarman PM, Payre F. From A to Z: apical structures and zona pellucida-domain proteins. Trends Cell Biol. 2010; 20(9):524–532. https://doi.org/10.1016/j. tcb.2010.06.002 PMID: 20598543

15. Gupta SK. The Human Egg's Zona Pellucida. Curr Top Dev Biol. 2018; 130:379–411. https://doi.org/10. 1016/bs.ctdb.2018.01.001 PMID: 29853184

16. Yan B, Zhang ZZ, Huang LY, Shen HL, Han ZG. OIT3 deficiency impairs uric acid reabsorption in renal tubule. FEBS Lett. 2012; 586(6):760–765. https://doi.org/10.1016/j.febslet.2012.01.038 PMID: 22306318

17. Legan PK, Rau A, Keen JN, Richardson GP. The mouse tectorins. Modular matrix proteins of the inner ear homologous to components of the sperm-egg adhesion system. J Biol Chem. 1997; 272(13):8791–8801. https://doi.org/10.1074/jbc.272.13.8791 PMID: 9079715

18. Op De Beeck K, Vermeire S., Rutgeerts P, Bossuyt X. Antibodies to GP2, the major zymogen granule membrane glycoprotein, in inflammatory bowel diseases. Gut. 2012; 61(1):162–164; author reply 164–165. https://doi.org/10.1136/gut.2010.233148 PMID: 21193445

19. Renner M, Bergmann G, Krebs I, End C, Lyer S, Hilberg F, et al. DMBT1 confers mucosal protection in vivo and a deletion variant is associated with Crohn's disease. Gastroenterology. 2007; 133(5):1499–1509. https://doi.org/10.1053/j.gastro.2007.08.007 PMID: 17983803

20. McAllister KA, Grogg KM, Johnson DW, Gallione CJ, Baldwin MA, Jackson CE, et al. Endoglin, a TGF-beta binding protein of endothelial cells, is the gene for hereditary haemorrhagic telangiectasia type 1. Nat Genet. 1994; 8(4):345–351. https://doi.org/10.1038/ng1294-345 PMID: 7894484

21. Wong SH, Hamel L, Chevalier S, Philip A. Endoglin expression on human microvascular endothelial cells association with betaglycan and formation of higher order complexes with TGF-beta signalling receptors. Eur J Biochem. 2000; 267(17):5550–5560. https://doi.org/10.1046/j.1432-1327.2000.01621. x PMID: 10951214

22. Cummings D, Cruise M, Lopez R, Roggenbuck D, Jairath V, Wang Y, et al. Loss of tolerance to glycoprotein 2 isoforms 1 and 4 is associated with Crohn's disease of the pouch. Aliment Pharmacol Ther. 2018; 48(11–12):1251–1259. https://doi.org/10.1111/apt.15034 PMID: 30411391

23. Mapes J, Li Q, Kannan A, Anandan L, Laws M, Lydon JP, et al. CUZD1 is a critical mediator of the JAK/STAT5 signaling pathway that controls mammary gland development during pregnancy. PLoS Genet. 2017; 13(3):e1006654. https://doi.org/10.1371/journal.pgen.1006654 PMID: 28278176

24. Wheeler E, Thomas S. Diagnosis and Long-term Management of Uromodulin Kidney Disease. Cureus. 2019; 11(3):e4270. https://doi.org/10.7759/cureus.4270 PMID: 31157132

25. Verhoeven K, Van Laer L, Kirschhofer K, Legan PK, Hughes DC, Schatteman I, et al. Mutations in the human alpha-tectorin gene cause autosomal dominant non-syndromic hearing impairment. Nat Genet. 1998; 19(1):60–62. https://doi.org/10.1038/ng0598-60 PMID: 9590290

26. Roggenbuck D, Hausdorf G, Martinez-Gamboa L, Reinhold D, Buttner T, Jungblut PR, et al. Identification of GP2, the major zymogen granule membrane glycoprotein, as the autoantigen of pancreatic antibodies in Crohn's disease. Gut. 2009; 58(12):1620–1628. https://doi.org/10.1136/gut.2008.162495 PMID: 19549613

27. Mustapha M, Weil D, Chardenoux S, Elias S, El-Zir E, Beckmann JS, et al. An alpha-tectorin gene defect causes a newly identified autosomal recessive form of sensorineural pre-lingual non-syndromic deafness, DFNB21. Hum Mol Genet. 1999; 8(3):409–412. https://doi.org/10.1093/hmg/8.3.409 PMID: 9949200

28. Lin SJ, Hu Y, Zhu J, Woodruff TK, Jardetzky TS. Structure of betaglycan zona pellucida (ZP)-C domain provides insights into ZP-mediated protein polymerization and TGF-beta binding. Proc Natl Acad Sci U S A. 2011; 108(13):5232–5236. https://doi.org/10.1073/pnas.1010689108 PMID: 21402931

29. Saito T, Bokhove M, Croci R, Zamora-Caballero S, Han L, Letarte M, et al. Structural Basis of the Human Endoglin-BMP9 Interaction: Insights into BMP Signaling and HHT1. Cell Rep. 2017; 19 (9):1917–1928. https://doi.org/10.1016/j.celrep.2017.05.011 PMID: 28564608

30. Bokhove M., & Jovine L. (2018). Structure of Zona Pellucida Module Proteins. Curr Top Dev Biol, 130, 413–442. https://doi.org/10.1016/bs.ctdb.2018.02.007 PMID: 29853186

31. Shen HL, Xu ZG, Huang LY, Liu D, Lin DH, Cao JB, et al. Liver-specific ZP domain-containing protein (LZP) as a new partner of Tamm-Horsfall protein harbors on renal tubules. Mol Cell Biochem. 2009; 321 (1–2):73–83. https://doi.org/10.1007/s11010-008-9921-3 PMID: 18830570

32. Wilburn DB, Swanson WJ. The "ZP domain" is not one, but likely two independent domains. Mol Reprod Dev. 2017; 84(4):284–285. https://doi.org/10.1002/mrd.22781 PMID: 28176401

33. Han L, Monne M, Okumura H, Schwend T, Cherry AL, Flot D, et al. Insights into egg coat assembly and egg-sperm interaction from the X-ray structure of full-length ZP3. Cell. 2010; 143(3):404–415. https://doi.org/10.1016/j.cell.2010.09.041 PMID: 20970175

34. Cohen JD, Flatt KM, Schroeder NE, Sundaram MV. Epithelial Shaping by Diverse Apical Extracellular Matrices Requires the Nidogen Domain Protein DEX-1 in Caenorhabditis elegans. Genetics. 2019; 211 (1):185–200. https://doi.org/10.1534/genetics.118.301752 PMID: 30409789

35. Bokhove M, Nishimura K, Brunati M, Han L, de Sanctis D, Rampoldi L, et al. A structured interdomain linker directs self-polymerization of human uromodulin. Proc Natl Acad Sci U S A. 2016; 113(6):1552–1557. https://doi.org/10.1073/pnas.1519803113 PMID: 26811476

36. Jovine L, Janssen WG, Litscher ES, Wassarman PM. The PLAC1-homology region of the ZP domain is sufficient for protein polymerisation. BMC Biochem. 2006; 7:11. https://doi.org/10.1186/1471-2091-7-11 PMID: 16600035

37. Louros NN, Chrysina ED, Baltatzis GE, Patsouris ES, Hamodrakas SJ, Iconomidou VA. A common 'aggregation-prone' interface possibly participates in the self-assembly of human zona pellucida pro-teins. FEBS Lett. 2016; 590(5):619–630. https://doi.org/10.1002/1873-3468.12099 PMID: 26879157

38. Louros NN, Iconomidou VA, Giannelou P, Hamodrakas SJ. Structural analysis of peptide-analogues of human Zona Pellucida ZP1 protein with amyloidogenic properties: insights into mammalian Zona Pellu-cida formation. PLoS One. 2013; 8(9):e73258. https://doi.org/10.1371/journal.pone.0073258 PMID: 24069181

39. Darie CC, Janssen WG, Litscher ES, Wassarman PM. Purified trout egg vitelline envelope proteins VEbeta and VEgamma polymerize into homomeric fibrils from dimers in vitro. Biochim Biophys Acta. 2008; 1784(2):385–392. https://doi.org/10.1016/j.bbapap.2007.10.011 PMID: 18067874

40. Litscher ES, Janssen WG, Darie CC, Wassarman PM. Purified mouse egg zona pellucida glycoproteins polymerize into homomeric fibrils under non-denaturing conditions. J Cell Physiol. 2008; 214(1):153–157. https://doi.org/10.1002/jcp.21174 PMID: 17559063

41. Monne M, Han L, Schwend T, Burendahl S, Jovine L. Crystal structure of the ZP-N domain of ZP3 reveals the core fold of animal egg coats. Nature. 2008; 456(7222):653–657. https://doi.org/10.1038/nature07599 PMID: 19052627

42. Williams Z, Wassarman PM. Secretion of mouse ZP3, the sperm receptor, requires cleavage of its poly-peptide at a consensus furin cleavage-site. Biochemistry. 2001; 40(4):929–937. https://doi.org/10.1021/bi002275x PMID: 11170414

43. Jimenez-Movilla M, Dean J. ZP2 and ZP3 cytoplasmic tails prevent premature interactions and ensure incorporation into the zona pellucida. J Cell Sci. 2011; 124(Pt 6):940–950. https://doi.org/10.1242/jcs.079988 PMID: 21378311

44. Jovine L, Qi H, Williams Z, Litscher ES, Wassarman PM. A duplicated motif controls assembly of zona pellucida domain proteins. Proc Natl Acad Sci U S A. 2004; 101(16):5922–5927. https://doi.org/10.1073/pnas.0401600101 PMID: 15079052

45. Boja ES, Hoodbhoy T, Fales HM, Dean J. Structural characterization of native mouse zona pellucida proteins using mass spectrometry. J Biol Chem. 2003; 278(36):34189–34202. https://doi.org/10.1074/jbc.M304026200 PMID: 12799386

46. Litscher ES, Qi H, Wassarman PM. Mouse zona pellucida glycoproteins mZP2 and mZP3 undergo car-boxy-terminal proteolytic processing in growing oocytes. Biochemistry. 1999; 38(38):12280–12287. https://doi.org/10.1021/bi991154y PMID: 10493795

47. Zhao M, Gold L, Dorward H, Liang LF, Hoodbhoy T, Boja E, et al. Mutation of a conserved hydrophobic patch prevents incorporation of ZP3 into the zona pellucida surrounding mouse eggs. Mol Cell Biol. 2003; 23(24):8982–8991. https://doi.org/10.1128/mcb.23.24.8982-8991.2003 PMID: 14645511

48. Brunati M, Perucca S, Han L, Cattaneo A, Consolato F, Andolfo A, et al. The serine protease hepsin mediates urinary secretion and polymerisation of Zona Pellucida domain protein uromodulin. Elife. 2015; 4:e08887. https://doi.org/10.7554/eLife.08887 PMID: 26673890

49. Fahrenkamp E, Algarra B, Jovine L. Mammalian egg coat modifications and the block to polyspermy. Mol Reprod Dev. 2020. https://doi.org/10.1002/mrd.23320 PMID: 32003503

50. Fernandes I, Chanut-Delalande H, Ferrer P, Latapie Y, Waltzer L, Affolter M, et al. Zona pellucida domain proteins remodel the apical compartment for localized cell shape changes. Dev Cell. 2010; 18 (1):64–76. https://doi.org/10.1016/j.devcel.2009.11.009 PMID: 20152178

51. Forman-Rubinsky R, Cohen JD, Sundaram MV. Lipocalins Are Required for Apical Extracellular Matrix Organization and Remodeling in Caenorhabditis elegans. Genetics. 2017; 207(2):625–642. https://doi.org/10.1534/genetics.117.300207 PMID: 28842397

52. Gill HK, Cohen JD, Ayala-Figueroa J, Forman-Rubinsky R, Poggioli C, Bickard K, et al. Integrity of Narrow Epithelial Tubes in the C. elegans Excretory System Requires a Transient Luminal Matrix. PLoS Genet. 2016; 12(8):e1006205. https://doi.org/10.1371/journal.pgen.1006205 PMID: 27482894

53. Kelley M, Yochem J, Krieg M, Calixto A, Heiman MG, Kuzmanov A, et al. FBN-1, a fibrillin-related protein, is required for resistance of the epidermis to mechanical deformation during C. elegans embryogenesis. Elife. 2015; 4. https://doi.org/10.7554/eLife.06565 PMID: 25798732

54. Low IIC, Williams CR, Chong MK, McLachlan IG, Wierbowski BM, Kolotuev I, Heiman M. G. Morphogenesis of neurons and glia within an epithelium. Development. 2019; 146(4). https://doi.org/10.1242/dev.171124 PMID: 30683663

55. Muriel JM, Brannan M, Taylor K, Johnstone IL, Lithgow GJ, Tuckwell D. M142.2 (cut-6):a novel Caenorhabditis elegans matrix gene important for dauer body shape. Dev Biol. 2003; 260(2):339–351. https://doi.org/10.1016/s0012-1606(03)00237-9 PMID: 12921736

56. Sapio MR, Hilliard MA, Cermola M, Favre R, Bazzicalupo P. The Zona Pellucida domain containing proteins, CUT-1, CUT-3 and CUT-5, play essential roles in the development of the larval alae in Caenorhabditis elegans. Dev Biol. 2005; 282(1):231–245. https://doi.org/10.1016/j.ydbio.2005.03.011 PMID: 15936343

57. Sebastiano M, Lassandro F, Bazzicalupo P. cut-1 a Caenorhabditis elegans gene coding for a dauer-specific noncollagenous component of the cuticle. Dev Biol. 1991; 146(2):519–530. https://doi.org/10.1016/0012-1606(91)90253-y PMID: 1864469

58. Vuong-Brender TTK, Suman SK, Labouesse M. The apical ECM preserves embryonic integrity and distributes mechanical stress during morphogenesis. Development. 2017; 144(23):4336–4349. https://doi.org/10.1242/dev.150383 PMID: 28526752

59. Yu RY, Nguyen CQ, Hall DH, Chow KL. Expression of ram-5 in the structural cell is required for sensory ray morphogenesis in Caenorhabditis elegans male tail. Embo J. 2000; 19(14):3542–3555. https://doi.org/10.1093/emboj/19.14.3542 PMID: 10899109

60. Corsi AK, Wightman B, Chalfie M. A Transparent window into biology: A primer on Caenorhabditis elegans. WormBook. 2015;1–31. https://doi.org/10.1895/wormbook.1.177.1 PMID: 26088431

61. Cohen JD, Sparacio AP, Belfi AC, Forman-Rubinsky R, Hall DH, Maul-Newby H, et al. A multi-layered and dynamic apical extracellular matrix shapes the vulva lumen in Caenorhabditis elegans. Elife. 2020; 9:e57874. https://doi.org/10.7554/eLife.57874 PMID: 32975517

62. Buechner M, Hall DH, Bhatt H, Hedgecock EM. Cystic canal mutants in Caenorhabditis elegans are defective in the apical membrane domain of the renal (excretory) cell. Dev Biol. 1999; 214(1):227–241. https://doi.org/10.1006/dbio.1999.9398 PMID: 10491271

63. Jones SJ, Baillie DL. Characterization of the let-653 gene in Caenorhabditis elegans. Mol Gen Genet. 1995; 248(6):719–726. https://doi.org/10.1007/BF02191712 PMID: 7476875

64. Pedelacq JD, Cabantous S, Tran T, Terwilliger TC, Waldo GS. Engineering and characterization of a superfolder green fluorescent protein. Nat Biotechnol. 2006 24(1):79–88. https://doi.org/10.1038/nbt1172 PMID: 16369541

65. Greenspan P, Mayer EP, Fowler SD. Nile red: a selective fluorescent stain for intracellular lipid droplets. J Cell Biol. 1985; 100(3);965–973. https://doi.org/10.1083/jcb.100.3.965 PMID: 3972906

66. Hawe A, Sutter M, Jiskoot W. Extrinsic fluorescent dyes as tools for protein characterization. Pharm Res. 2008; 25(7):1487–1499. https://doi.org/10.1007/s11095-007-9516-9 PMID: 18172579

67. Sackett DL, Wolff J. Nile red as a polarity-sensitive fluorescent probe of hydrophobic protein surfaces. Anal Biochem. 1987; 167(2):228–234. https://doi.org/10.1016/0003-2697(87)90157-6 PMID: 3442318

68. Weadick CJ. Molecular evolutionary analysis of nematode Zona Pellucida (ZP) modules reveals disulfide-bond reshuffling and standalone ZP-C domains. Genome Biol Evol. 2020;. https://doi.org/10.1093/gbe/evaa095 PMID: 32426804

69. Stanisich JJ, Zyla DS, Afanasyev P, Xu J, Kipp A, Olinger E, et al. The cryo-EM structure of the human uromodulin filament core reveals a unique assembly mechanism. Elife. 2020; 9.e60265. https://doi.org/10.7554/eLife.60265 PMID: 32815518

70. Stsiapanava A, Xu C, Brunati M, Zamora-Caballero S, Schaeffer C, Han L, Carroni M, et al. Cryo-EM Structure of Native Human Uromodulin, a Zona Pellucida Module Polymer. BioRxiv. 2020. https://doi.org/10.1101/2020.05.28.119206

71. Diestel U, Resch M, Meinhardt K, Weiler S, Hellmann TV, Mueller TD, et al. Identification of a Novel TGF-beta-Binding Site in the Zona Pellucida C-terminal (ZP-C) Domain of TGF-beta-Receptor-3 (TGFR-3). PLoS One. 2013; 8(6):e67214. https://doi.org/10.1371/journal.pone.0067214 PMID: 23826237

72. Smith SJ, Davidson LA, Rebeiz M. Evolutionary expansion of apical extracellular matrix is required for the elongation of cells in a novel structure. Elife. 2020; 9. https://doi.org/10.7554/eLife.55965 PMID: 32338602

73. Raj I, Sadat Al Hosseini H, Dioguardi E, Nishimura K, Han L, Villa A, et al. Structural Basis of Egg Coat-Sperm Recognition at Fertilization. Cell. 2017: 169(7), 1315–1326.e1317. https://doi.org/10.1016/j.cell.2017.05.033 PMID: 28622512

74. Brenner S. The genetics of Caenorhabditis elegans. Genetics. 1974; 77(1):71–94. PMID: 4366476

75. Dodt HU, Zieglgansberger W. Visualizing unstained neurons in living brain slices by infrared DIC-video-microscopy. Brain Res. 1990; 537(1–2);333–336. https://doi.org/10.1016/0006-8993(90)90380-t PMID: 2085783

76. Bidaud-Meynard A, Nicolle O, Heck M, Le Cunff Y, Michaux G. A V0-ATPase-dependent apical trafficking pathway maintains the polarity of the intestinal absorptive membrane. Development. 2019; 146(11). https://doi.org/10.1242/dev.174508 PMID: 31110027

77. Nance J, Frøkjær-Jensen C. The Caenorhabditis elegans Transgenic Toolbox. Genetics. 2019; 212 (4):959–990. https://doi.org/10.1534/genetics.119.301506 PMID: 31405997

78. Reits EA, Neefjes JJ. From fixed to FRAP: measuring protein mobility and activity in living cells. Nat Cell Biol. 2001; 3(6):145–147. https://doi.org/10.1038/35078615 PMID: 11389456

79. Yanagawa S, Lee JS, Ishimoto A. Identification and characterization of a novel line of Drosophila Schneider S2 cells that respond to wingless signaling. J Biol Chem. 1998; 273(48):32353–32359. https://doi.org/10.1074/jbc.273.48.32353 PMID: 9822716

80. Stiernagle T. Maintenance of C. elegans. WormBook. 2006;1–11. https://doi.org/10.1895/wormbook.1.101.1 PMID: 18050451

81. Tordai H, Banyai L, Patthy L. The PAN module: the N-terminal domains of plasminogen and hepatocyte growth factor are homologous with the apple domains of the prekallikrein family and with a novel domain found in numerous nematode proteins. FEBS Lett. 1999; 461(1–2):63–67. https://doi.org/10.1016/s0014-5793(99)01416-7 PMID: 10561497

82. Kyte J, Doolittle RF. A simple method for displaying the hydropathic character of a protein. J Mol Biol. 1982; 157(1):105–132. https://doi.org/10.1016/0022-2836(82)90515-0 PMID: 7108955